2011-01-01

Magnetic-Field Induced Stability in Two-Flavor Color Superconductivity

Churna B. Bhandari
University of Texas at El Paso, cbhandari81@gmail.com

Magnetic-Field Induced Stability in Two-Flavor Color Superconductivity

Churna Bahadur Bhandari

Department of Physics

APPROVED:

Vivian Incera, Ph.D., Chair

Efrain Ferrer, Ph.D.

Cristina Mariani, Ph.D.

Patricia D. Witherspoon, Ph.D.
Dean of the Graduate School

Magnetic-Field Induced Stability in Two-Flavor Color Superconductivity

By

Churna Bahadur Bhandari

Thesis

Presented to the Faculty of the Graduate School of

The University of Texas at El Paso

in Partial Fulfillment

of the Requirements

for the Degree of

Master of Science

Department of Physics

THE UNIVERSITY OF TEXAS AT EL PASO

May 2011

Acknowledgements

I would like to express my sincere gratitude to my supervisor Prof. and Chair Vivian Incera for her proper suggestion and guidance for the completion of this research work. Her timely assistance and valuable suggestions have been of immense value.

I would also like to express my sincere gratitude to Prof. Efrain Ferrer for his helpful suggestions and advices during the course of this work.

I would like to thank Dr. Hikmat B.C., Dr. Pheng Bo and Dr. Angel Sanchez for their valuable suggestions and ideas during this work.

I am also very grateful with my parents and brothers who have supported me and provided their continuos encouragement and feedback.

Finally, I would also like to acknowledge UTEP for its financial support and warm hospitality to pursue my education and complete my research work.

Abstract

It has long been understood that the ground state of a superdense quark system, a Fermi liquid of weakly interacting quarks, is unstable with respect to the formation of diquark condensates. This nonperturbative phenomenon is essentially equivalent to the Cooper instability of conventional BCS superconductivity. As the quark pairs have nonzero color charge, this kind of superconductivity breaks the SU(3) color gauge symmetry, thus it is called color superconductivity. A peculiar feature of spin-zero color superconductivity is the lack of Meissner effect for a combination of the regular electromagnetic field and one of the gluon fields. This combination behaves as an in-medium electromagnetic field and as a consequence, a regular magnetic field can penetrate the color superconductor through its long-range in-medium component. Since the conditions of very high dense matter and very strong magnetic fields are naturally found in neutron stars, the investigations of magnetic field effects in color superconductivity are relevant for astrophysics. In this work we investigate the effects of an external magnetic field in the stability of the ground state of a neutral two-flavor color superconductor. Our results show that a strong magnetic field tends to increase the stability of the ground state, moving it from the unstable gapped region to the stable one.

Table of Contents

List of Figures

Chapter 1

Introduction

Matter is composed by atoms. The atoms consist of a cloud of electrons surrounding a densely-packed nucleus of protons and neutrons. Protons and neutrons are heavy particles called baryons. Their masses are nearly 1800 times that of the electron. These massive baryons are confined in a tremendously small volume within an atom called a "nucleus", which is of the size of the order 10^{-15} m. The density, therefore, of a nucleus(nuclear matter) is extraordinarily large compared to atomic matter. For instance, the size of a penny, composed solely of nuclear matter, would weigh five billion tons. Still there are other settings in nature where the density may be as large as ten times that within the nuclei of atoms. The matter of such density is believed to be found in the central regions of compact stellar objects known as neutron stars. It has been believed that baryonic matter is more densely packed in those settings than in nuclei. As a consequence, it loses its structure altogether, and becomes what we call quark matter.

The overwhelming motivation of this thesis is to better understand the way quark matter behaves in the presence of a magnetic field. Particularly, we consider the regime of very low (effectively zero) temperature, and very large density, but not asymptotically so. Of course, the zero temperature here is good to describe the situation where the density of quark matter is very large compared to the

temperature like in the case of a neutron star. This sufficiently cold and dense quark matter is a color superconductor [1]. Here, we take up mainly a two-flavor color superconductivity(referred to 2SC) based on the Nambu-Jona-Lasinio (NJL) model to give a possible description of quark matter. Our main focus is to discuss the effects of magnetic field on 2SC color superconductivity. In the following sections of this chapter, we discuss some basic ideas of cold and dense quark matter, quarks and QCD, and QCD phase diagram and chromomagnetic instability. In chapter 2, we review the general concepts underlying conventional superconductivity. After covering these pertinent ideas from the chapter 2, we discuss the color superconductivity in absence of a magnetic field in chapter 3 and in presence of a magnetic field in chapter 4. In chapter 5, we discuss the results of this work.

1.1 Quark and QCD

Baryons are composed of more basic particles called quarks. The quarks are known to be fundamental particles; that is, they are not made up of smaller components and have no internal structure. The quarks come in six flavors such as: down(d), up(u), strange(s), charm(c), bottom(b), top(t). The up and down quarks are known to be the first generation, and the next two pairs make up the more massive second and third generations respectively. For each quark, there exists a corresponding anti-particle(anti-quark). For example, the anti quark of up(u) is denoted by a $\bar{u}$.

The u, d, and s are the lightest quarks known in the nature. At realistic densities, these are the most likely to be present in quark matter. In our discussion of color superconductivity below, we will consider only two u and d quarks. The u and

d quarks have a bare, mass of $m_{u,d} \sim 5$ MeV and the medium-weight strange quark has a current mass of $m_s \sim 100$ MeV. But the effective constituent masses, $M_{u,d,s}$, are apparently larger, of the order of hundreds of MeV. These constituent quark masses are supposed to be density dependent, decreasing with increasing quark density.

Unlike the electron which possesses only electric charge, quarks carry fractional electric as well as color charge. The first and second members of each generation has $-\frac{1}{3}$ and $+\frac{2}{3}$ electric charge respectively. There are three color charges associated with each quark, often denoted red, green, and blue. Quarks of each flavor have internal degrees of freedom associated to these color charges. The notation here for color labels an internal quantum state which quarks possess and is not related to the color in the common sense of hues.

There is a strong interaction between quarks mediated by a gauge particle called gluons. The gluons are elementary particles which act as exchange particles(or gauge bosons) for the color force between quarks, analogous to the exchange of photons in the electromagnetic force between two charged particles. The strong interaction which occurs due to the exchange of gluons between quarks, is described by the theory known as Quantum Chromodynamics (QCD). This gauge theory is essentially based on the color symmetry group $SU(3)_C$. One of the unique feature of gluons in QCD is that they themselves carry color (one charge, one anti-charge) and so interact with one another. Associated with this is a remarkable property with strong interaction known as confinement, which says that quarks must be confined into collections that are color-neutral. This implies that an isolated, free quark can never be observed in nature. Quarks, therefore, form colorless pairs and triplet-mesons and baryons respectively collectively known as hadrons. Mesons are made up of a quark of one color and an anti quark of the

corresponding anti color. For example, a π^+ meson, is built up by a red u quark and an anti-red d quark. The baryons are made of three quarks, each of different colors forming a color-neutral composite. For example, a proton is a composite of two u quarks and one d quark.

The color of quarks is associated to the fundamental representation (3) of the color symmetry group, $SU(3)_C$. The quarks are introduced as spinor fields in N_f flavors, each in the fundamental representation (triplet, denoted 3) of the color gauge group, $SU(3)$. This is an exact symmetry and the strong interaction coupling is independent of the choice of the particular color. The gluons are vector fields in the adjoint representation (octets, denoted 8) of color SU(3). For a general gauge group, the number of force-carriers (like photons or gluons) is always equal to the dimension of the adjoint representation i.e., $3^2 - 1 = 8$ color combinations.

As gluons possess intrinsic property, the color, it makes QCD a complicated non-Abelian gauge theory. The strength of quark-gluon interaction is given by a coupling constant α_s, whose value depends on the energy scale of the system of the quark matter. At finite density ρ of quarks and zero temperature, that energy scale is determined by the baryon chemical potential μ, which in turn is related to quark density $\rho \propto \mu^3$. Then, at finite density μ sets the QCD coupling i.e., $\alpha_s \sim \alpha_s(\mu)$. This hallmarks the important feature of QCD known as asymptotic freedom. Quarks become nearly free as their density (and/or temperature) becomes asymptotically large [2]. Thus at higher densities, or chemical potentials, quarks interaction gets weaker.

1.2 Quark Matter

1.2.1 The QCD Phase Diagram

The study of matter at extremely high densities has sometimes also been termed as "the condensed matter physics of QCD" [1]. The reason for this is the analogy existing between many phenomena known in condensed matter and the behavior of quarks at high densities. Of particular interest for this thesis is the analogy between conventional electric superconductivity which occurs in metals, ceramics and other materials, and color superconductivity that occurs only in dense quark matter.

The thermodynamic behaviors of a system are conveniently displayed in terms of a phase diagram. The QCD schematic phase diagram is shown in Fig.1.1, which refers to the $\mu - T$ plane. Here, each point on the diagram corresponds to a quark-gluon system in a certain thermodynamic state, occurring at particular values of the quark chemical potential μ and temperature T. The system is considered to be infinitely large and each state as one in thermal equilibrium.

To date, QCD at the regime of asymptotically high density or asymptotically high temperature is better understood. As mentioned in earlier section, at asymptotically high densities, the coupling $\alpha_s(\mu)$ is small, thus the theory becomes workable analytically, and calculations can be made more rigorously from first principles [3]. Such calculations, as well as effective model calculations, have shown that, the phase structure of quark matter is richly diverse similar to that of ordinary condensed matter physics.

Generally speaking, QCD phase diagram as shown in Fig.1.1, is much more complicated than that of a normal thermodynamical system. The QCD diagram still

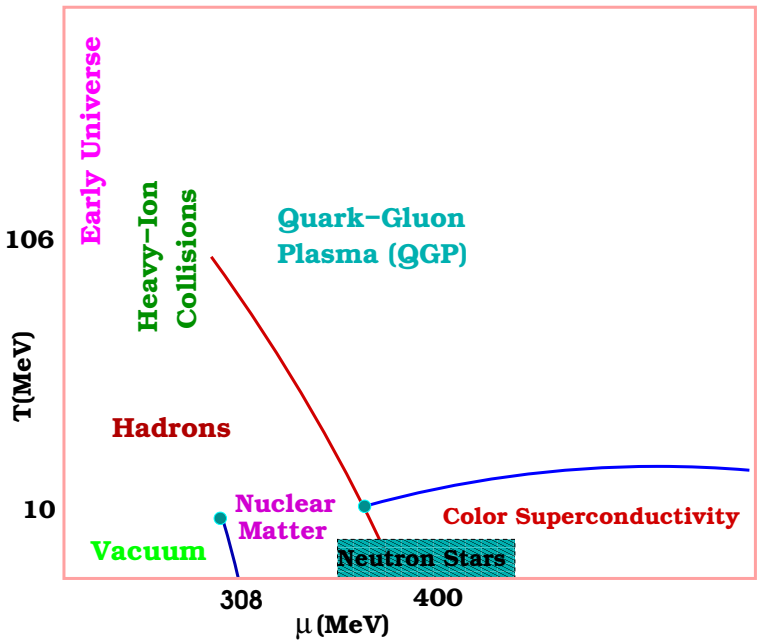

Figure 1.1: Schematic view of the QCD phase diagram indicating the phase boundaries of various transitions.

needs more clarification in regards to the various transitions. For example, it is neither yet reliably understood where in the diagram the transition from hadronic to quark matter occurs nor known whether or not this deconfinement is a true phase transition, as there is no symmetry related order parameter [4]. In addition to these, we will notice that for the cold and intermediately dense portion of the diagram, many quark matter phases have been proposed. Although great efforts have been made, it still remains an outstanding problem which of these phases are realized in nature.

Recent years, there has been much focus in those parts of the QCD phase diagram for which either the temperature or density becomes tremendously large, i.e., asymptotically free regimes. The works are being done to better understand the picture beyond the hadronic phase in both experimental and theoretical fronts. The final hope is to have a clear and complete picture of the QCD phase diagram,

describing at each density and temperature the form in which quark matter occurs.

Depending on the temperature T and quark chemical potential μ, quark matter has several different phases as shown in Fig.1.1. Along the vertical axis $\mu = 0$ MeV, the temperature increases, taking us through the crossover from a hadronic gas to the quark-gluon plasma at some finite T. The hadronic regime occurs at low temperatures and densities. At the quark-gluon plasma (QGP) regime ($T >> \mu$), there is asymptotic freedom and therefore in this novel form of matter, quarks and gluons are nearly free and both have their color charges unscreened. The entropy associated with QGP is very large at high temperatures, therefore there is no spontaneous symmetry breaking; that is, there are no phase transitions [3]. At low temperatures, $T << \mu$, varieties of quark pairing patterns are thought to fill the high density landscape of the QCD phase diagram [5]. This is the region of color superconducting phases, in which Cooper pairs of quarks are formed at the Fermi surface. The physics underlying Cooper pairs will be discussed in Chapter 2. There have been several color superconducting phases introduced recently.

The quark matter at highest densities i.e., ($\mu >> T \sim$ or$M_{u,d,s}$), is expected to be a color superconductor in the color-flavor locked (CFL) phase [6]. Here, massless up, down, and strange quarks of all three colors are paired in the most symmetric manner available. In this case, constituent masses are approximately equal to the current masses, which are negligible compared to densities [6, 7, 8]. As the strange quark constituent mass M_s is much greater than the up and down masses, it plays a significant role in deciding which color superconducting phases are physically viable. As we discussed earlier, the dynamically generated constituent masses are thought to rely on the density, or chemical potential, $M \sim M(\mu)$. For very large μ, the strange quark becomes essentially massless

and can readily participate in pairing with u and d quarks. As we go to regime where the density is effectively low, however, the strange quark mass increases and becomes comparable to the quark chemical potential at some densities. In neutron stars, for example, the chemical potential is not likely to be greater than 500 MeV, while the constituent mass of the strange quark is somewhere between its current mass (100 MeV) and its vacuum constituent mass (500 MeV) [4]. At intermediate densities, then, M_s is no longer negligible. At this condition the strange quark may not be energetically favorable to pair with the light up and down quarks. The strange quarks therefore may not appear in the Cooper pairing at moderate densities.

From what it follows that the CFL condensate may not reflect the true ground state of quark matter at intermediate densities. In that case, less symmetrically paired forms of quark matter will come into play. According to the work done in [5] the next phase down in density will be gapless CFL. They also argue that a continuous transition from CFL to gapless CFL will take place at $\frac{M_s^2}{\mu} \approx 2\Delta$, where Δ is the gap parameter. Gapless CFL, however, is found to be unstable. Other phases, for instance kaon CFL and crystalline color superconductors, have also been studied as well for densities lower than that of CFL.

Because of the potentially large strange quark mass, one may expect that there may exist two-flavor color superconducting phase. The 2SC phase, where massless up and down quarks of two colors pair, is the state we consider in this work. We study the effects of a magnetic field on this two-flavor phase and discuss how the large magnetic field creates stability in that phase.

Before entering to the color superconductivity and the 2SC pattern in a magnetic field, we review physics behind conventional superconductivity in chapter 2, which involves electrons in a cold metal, rather than quarks in a compact star.

Many of these concepts from the normal superconductivity will make easier to follow the study of quark matter.

Chapter 2

Conventional Superconductivity

2.1 General Considerations

Before entering in to the topic of color superconductivity, it is better to give a summary of the phenomenon of conventional superconductivity. This will be a natural and convenient way to transit from conventional to color superconductivity making it easier to understand this phenomenon in the QCD context. Here we discuss some salient features of electric superconductors.

2.2 The Normal Metals

A metal consists of a positive-ion core immersed in a sea of conduction electrons. The conduction electrons are considered to be a non-interacting Fermi gas. According to Pauli exclusion principle no two fermions (spin $-\frac{1}{2}$) can have the same quantum state. Within this framework, the system of free electrons is considered as the quantum mechanical version of an ideal gas. At the macroscopic level, the ground state of the many-electron system will be a stack of single-particle states, beginning with the lowest energy state and building up to the topmost occupied level. At 0 K, Fermi gas at ground state fills up to a topmost occupied level. This

topmost occupied level is called Fermi level and the energy is the Fermi energy, ϵ_F.

For the Fermi gas the potential energy is zero. Therefore the energy of free single particle state k ϵ_k is given by

$$\epsilon_k = \frac{p^2}{2m}$$

where m is the mass of and $p = \hbar k$ is momentum of electron, k wave vector.

$$\epsilon_k = \frac{\hbar^2 k^2}{2m} = \frac{\hbar^2}{2m}(k_x^2 + k_y^2 + k_z^2) \tag{2.1}$$

where $k_i (i = x, y, z)$ are the components of $\vec{k}$. The single particle state therefore can be represented by a point in k space. Even though stacking of single particle energy occurs in real space, we can still view stacking of energy level in a volume of momentum space(k space) for the easier understanding. Because of the spherical symmetry, the system of the free electron gas in the ground state fills up to the topmost level comprising a sphere of radius k_F, where $\epsilon_F = \frac{\hbar^2 k_F^2}{2m}$. This is so-called Fermi sphere, or Fermi sea. The surface of Fermi sea is known as Fermi surface.

2.2.1 The Fermi-Dirac Distribution

As mentioned above, all the single particle states are filled up to Fermi surface at zero temperature,. When the temperature of the system increases, the electrons close to that Fermi level get excited due to thermal energy. At the same time, the occupied level below the Fermi surface becomes empty. Thus, at finite temperature the distribution of conduction electrons is smeared around Fermi level. The occupation number for the electron at energy level ϵ is given by so-called

Fermi-Dirac distribution which gives the probability that a single-particle sate of energy ϵ will be occupied at temperature T. The Fermi-Dirac distribution is

$$f(\epsilon) = \frac{1}{e^{\frac{(\epsilon-\mu)}{k_B T}} + 1} \tag{2.2}$$

where $\mu = \mu(T)$ is the chemical potential, which depends on the temperature, and k_B is Boltzmann constant.

The chemical potential is the energy added or lost while adding or removing a single particle from a stack of energy levels. At zero temperature the chemical potential is $\mu(0) = \epsilon_F$.

The Fermi-Dirac distribution at zero temperature behaves like a step function: it is 1; for all ϵ up to ϵ_F and abruptly falls to zero otherwise. At nonzero temperature, it smears around the Fermi energy. It follows from the fact that as we raise the temperature, only those electrons lying on the states beneath the Fermi surface are excited to states just above the Fermi energy. This lowers the occupation number of single particle states at the vicinity of Fermi energy.

This smearing of electrons at the neighborhood of Fermi energy is due to the large size Fermi energy and the Pauli principle. The Fermi energy of metals is typically of the order of a few electron volts which is very large compared to ordinary electron interactions. For example, Copper has a Fermi energy of 7 eV. The amount of energy available as a result of the temperature is of the order of the average thermal energy, for which $k_B T = 00.026$ eV at room temperature i.e., 300 K [9].

A fact of Pauli principle is that the majority of electrons beneath the Fermi surface cannot receive energy from these interactions since all states within a fraction of an electron volt are already occupied. In terms of available quantum states,

these electrons have no states to go to i.e., they are Pauli blocked. A state deep inside the Fermi sea would therefore require a thermal energy of order eV to get excited above the Fermi surface to an available state.

2.2.2 The Electron-Phonon-Electron Interaction

Even in normal temperature, the electrons within the shallow depth of k_BT beneath the surface get excited above Fermi level. At this temperature, the electrons further down in the sea neither have sufficient thermal energy to escape above Fermi sea nor is there available states for them to go to within deep down to the Fermi surface. At the vicinity of the Fermi surface, however, the kinetic energy of the conduction electrons is increased with a small rise in the temperature. Due to this raised thermal kinetic energy those electrons get excited to higher states. This would still occur even in the absence of metal lattice. Another excitation may result from collisions between conduction electrons and the lattice. When the temperature increases so does the lattice vibration. The energy spectrum of a lattice vibration is normally quantized, and the quantum of energy is called a phonon. The waves associated with these phonons are elastic waves. Due to the vibration of phonons there is a sort of instability in lattice structure. On the other hand this effect is sensed by the conduction electrons. The effective attractive interaction between two electrons is mediated by phonons [9]: Electron-phonon collisions scatter the electron from state k to state $k^{'}$, leading to electrical resistance. The ion-electron attraction causes a distortion in the lattice, which effectively screens the electron charge. This distortion of one electron is experienced by a second electron, thereby causing the electron-electron interaction that enters in the theory of superconductivity.

We know that electrical resistance is an intrinsic property of metals. Normally

in most metals, the electrical resistance is dominated at room temperature by collisions of the conduction electrons with lattice phonons [9]. These collisions bring the electrons into a scattered, or resisted state which results in resistance in metals. One can also notice that resistance may develop only if the conduction electrons are interacting with the lattice. Such interactions are not included in the free electron picture.

In the free electron model, there is a continuum of energy spectrum in metals. When interactions are also included into this model, one can see that the available electron energies are arranged in a continuous conduction band. From band structure calculations many properties of the metals are explored [9]. As the metal conduction band is continuous, there is no minimum energy required to scatter an electron at the Fermi level to an excited state. Even a very small amount of thermal energy will be enough to raise an electron at the Fermi surface to a scattered state just above the surface. Thus, in a perfectly pure sample, we expect to have scattering and hence resistance at all temperatures except 0K. However, in the presence of impurities in the lattice, a resistance beyond that of phonon scattering develops even at zero temperature. We therefore would not expect the resistance falling to zero at any temperatures in impure samples.

2.3 The Superconducting State

After the first liquidification of helium in 1908, the Dutch physicist Kamerlingh Onnes began cooling certain pure metals to temperatures near 4 K and observing their conduction properties. He wanted to know how the conduction electrons would behave at exceedingly low temperatures. In 1911, Onnes discovered that at 4.2 K the resistance of the metal abruptly dropped and became immeasurably

small.

Further efforts also showed that several other materials display this behavior at a certain critical temperature, T_c , the resistance falls sharply to zero, and remains zero for all temperatures below T_c. At a temperature below T_c , the material will carry a current called persistent current which will last indefinitely, conducting without any dissipation. Such materials are known as superconductors.

As mentioned above, the normal ground state fills a sea of electron energy levels up to the Fermi surface, above which lies a continuous availability of states. These available states allow electrons to have resistance at any nonzero temperature, as there exist higher energy levels to which electrons may be scattered when receiving energy from the lattice. If in some way in the superconducting ground state, a strip of energy levels above the Fermi surface could be removed, then there would be no resistance since states available for scattering would be absent. This would be possible at low temperatures, where this gap in allowed energies could be more than the electron scattering energy. The gap would prevent the scattering of electrons into the next higher states at any temperatures below T_c. If such a gap in the electron energies could be explained theoretically, it could explain Onnes finding of mercury entering a zero-resistance state at a non-zero temperature. To explain Onnes discovery in 1911, several phenomenological theories were proposed which attempted to capture the essential features of superconductivity. It took nearly half century for theorists to get a complete and accurate picture to understand the fundamental physics of the gap. This theoretical understanding was made by Bardeen, Cooper, and Schrieffer in 1957, when they put forward their BCS Theory [10].

2.3.1 The BCS Ground State

In the microscopic BCS theory, the energy gap follows from the pairing of electrons near the Fermi surface. This pairing mechanism was first studied by Leon Cooper, who initially considered a single pair of electrons interacting above a non-interacting Fermi sea [11]. He found that there exists a bound state of two electrons for arbitrarily weak coupling as long as the potential is attractive near the Fermi surface. Such a bound state of two electrons is known as a Cooper pair.

Given the Coulomb repulsive interaction between electrons, the way by which Cooper pairs are formed was not clear at that moment. However, an effective attraction between electrons takes place when one electron interacts with the lattice and deforms it; a second electron sees the deformed lattice and adjusts itself to take advantage of the deformation to lower its energy. Therefore, the mates of a pair can interact by way of this lattice deformation. Cooper pairing is thus possible thanks to an electron-electron interaction mediated by a phonon.

In other words, the electrons in a Cooper pair are bound together by this attractive interaction. There is a finite amount of energy required to break them apart. This is the energy needed for single-particle excitation at the Fermi surface and is called the superconducting energy gap, Δ. The presence of such a gap leads to a finite-temperature ordered state with zero resistance, as small excitations, such as scattering, are not able to excite electrons to states above the gap.

According to the BCS theory, the gap equation for a system with temperature T and chemical potential μ is given by

$$\Delta_k = g \int \frac{\Delta_k d^3k}{(2\pi)^3} \tanh(\frac{E_k}{2k_B T}) \tag{2.3}$$

where, k_B is the Boltzmann constant, g the coupling constant of the effective electron- electron interaction, and E_k the energy spectrum of Bogoliubov quasiparticles. For a particle with energy ϵ_k^0, the dispersion relation is given by

$$E_k = \sqrt{(\epsilon_k^0 - \mu)^2 + \Delta_k^2} \tag{2.4}$$

For a particle with $k = k_F$, $\epsilon_k^0 = \mu = \epsilon_F$, the excitation energy is simply equal to gap.

The Eq.2.3 is a nonlinear integral equation for a whole unknown function Δ_k, which in general could only be solved by numeric integration. Since the actual pairing potential hardly depends up on wave vectors at all: the electrons at k and $k^{'}$ feel an attraction of about same strength, provided that $\mid \epsilon_k - \epsilon_{k'} \mid < \hbar\omega_c$, where ω_c is the Debye cutoff frequency characteristic of metals and $\hbar\omega_c$ is the Debye cutoff energy. Hence $\Delta_k = \Delta$ up to the cutoff k and zero else where. We can then factor out the Δ from the integral and the integral can be evaluated easily. After simplification, at absolute temperature the gap takes the following form

$$\Delta = 2\hbar\omega_c \exp(-\frac{1}{N_F g}) \tag{2.5}$$

where

$$N_F = \frac{mk_F}{2\pi^2\hbar^2} \tag{2.6}$$

is the density of states at Fermi surface. The structure of the gap given by Eq. 2.5, with the coupling multiplying the density of states in the exponential, is a consequence of the BCS theory. We will revisit this concept in the context of color superconductivity when discussing the CFL and 2SC gaps.

As we mentioned above, the strength of the attraction between pairing electrons

is smaller than than Debye cutoff energy. This is equivalent to saying that there is an exchange of a virtual phonon, whose momentum is much smaller than $\hbar k_F$. Due to the Pauli blocking, only electrons at the vicinity of the Fermi surface, say, in an interval $[k_F - q, k_F + q]$, where $q << k_F$ is determined by the Debye energy, can interact via this phonon exchange. This is the reason why Cooper pairs are bound to the Fermi sphere unlike free electrons which are bound to lattice and the phenomenon is a pure Fermi surface phenomenon.

The superconducting ground state has a lower free energy than that of the filled Fermi sphere by the amount of the sum of binding energies of the Cooper pairs. Therefore it creates the famous Cooper instability of the normal ground state. At low temperatures, Cooper pairs condense to the energetically favored BCS ground state. This pair condensate marks the presence of an ordered phase i.e., superconductivity.

2.3.2 Meissner Effect

A type I superconductor expels out all field lines when placed in a weak external magnetic field. Except from a shallow depth to which the field does penetrate, a magnetic field cannot enter deep inside a superconductor. This is called the Meissner effect, first noted by Meissner and Ochsenfeld in 1933. This diamagnetic behavior, as well as the zero resistivity are key features of conventional superconductors.

The diamagnetic behavior of a superconductor arises from screening currents which move over the surface of the material. These currents produce a magnetic field which perfectly opposes the applied field. The description of the Meissner effect can also be given in terms of a spontaneous breaking of symmetry. The Cooper pairs form a electrically charged condensate thereby breaking the $U(1)_{em}$

gauge symmetry of electromagnetism. The photon acquires an effective mass, referred to as its Meissner mass, and so it cannot penetrate the material.

If the applied magnetic field is greater than a critical value H_c, the superconducting state is disrupted and the normal state sets in. This transition from the superconducting to the normal state is different depending upon the varieties of superconductor type I and type II.

In the type I superconductor, there is an abrupt change from the superconducting to the normal state at a critical value of the external field. For a given temperature below T_c , superconductivity is destroyed once the magnetic field exceeds H_c. This critical field is temperature-dependent, larger at lower temperatures where superconductivity is strongest, and reaching zero at T_c.

The second type of superconductors are characterized by two critical fields and the transition from the Meissner state is smooth. For an applied field below the first critical value H_{c1}, the superconducting state holds. Above the second field H_{c2} resides the normal state. In between these critical field values, a mixed state exists in which tubes of magnetic flux pierce the superconducting material [9], the so-called vertex state.

Chapter 3

Color Superconductors

3.1 General Consideration

In this chapter, we discuss briefly about color superconductivity. In recent years there has been significant progress in the study of dense quark matter. Of particular interest is the state of any dense and cold quark matter, which should be in some phase of color superconductivity. In order to describe color super conductivity we can connect it with the basic physics presented in the previous chapter.

A fundamental difference that we need to consider is a non-relativistic to a relativistic treatment. Nevertheless, the basic mechanism is still described by Cooper's pair formation. What one has to do is to replace the electron liquid, interacting via exchange of virtual phonons, by a quark-gluon interacting via the strong interaction, which is embedded in the Lagrangian of QCD, hence, no lattice is required for color superconductivity. Due to asymptotic freedom, the strong interaction at (asymptotically) high densities is dominated by the exchange of a single gluon. And indeed, there is an attractive channel for this interaction, providing the conditions for the application of the Cooper theorem. Consequently, for temperatures low compared to the baryon density, the quarks at their Fermi

surface rearrange in order to form a ground state characterized by the existence of quark Cooper pairs [6, 12, 13].

It has long been known that at large energy scales the quark-gluon interaction becomes weak. This ultrarelativistic behavior of QCD is known in the literature as asymptotic freedom [2]. The asymptotic freedom can occur at very high temperatures, as in the early universe, and also at very high densities, as those in the core of a neutron star. The initial work regarding the formation of quark Cooper pair was done in [12, 14], where they first coined the name "color-superconductivity." Details of the pairing mechanism and numerical calculations were then given in [12, 15]. Using perturbation method, it was found that single-gluon exchange brought about pairing of gaps of order 1 MeV which is too small to have observable effects compared to the energy scale of the order 100 MeV. From this method of perturbative iterations, the signature of color superconductivity could not come to be an observable phenomena.

In the last decades, new nonperturbative methods have been devised to calculate quark pairing gaps. These calculations showed that the diquark condensate could be of the order of 100 MeV at densities that could exist in the interior of compact stars[6, 16]. Since the prediction of these sizable gaps, the demonstration of the stable CFL phase [6] has already been well established. Still the question what happens to quark matter when it is compressed to arbitrary densities has not been fully understood due to instabilities occurring at more realistic, intermediate densities. Since quark carry a color degree of freedom, the pairing of two quarks cannot be a color singlet. The Cooper pairs therefore break the local color symmetry $SU(3)_C$, giving rise to color superconductivity. At asymptotic densities weak-coupling calculations can be made from first principles. In addition to this, the ratio of gap and Fermi energy is greater than in conventional super-

conductivity. Unlike conventional superconductivity where the effective phonon interaction which causes pairing of fermions requires a complicated band structure calculations in lattice, calculations of color superconductivity is straight-forward in QCD.

In the case of color superconductor, there are many theoretically possible phases which merely depends on the number of quark flavors N_f present on the system. In the next following sections, we briefly review 3- and 2-flavor color superconductors. In addition to these, we also discuss some physical observables from which we can describe the phenomena of color superconductivity.

3.2 Two and Three Flavor Color Superconductors

3.2.1 Two Flavor Color Superconductor

Two-flavor color superconductivity is important when the density is not large enough and the strange quark mass is comparable to the density, so strange quark cannot be excited. In this case, only the two lightest flavors, u and d, become important. In the case of two flavor color superconductor, the Cooper pairs are formed by pairing of two of three flavors and two of three colors. Hence, the massless quarks u and d are only one contributing to the formation of pairs. This phase of color superconductor is known as "2SC phase." Red and green are conventionally considered as the colors included in the pairing. All blue quarks therefore remain unpaired. The original symmetry

$$G = SU(3)_C \otimes SU(2)_L \otimes SU(2)_R \tag{3.1}$$

is broken to

$$H_{2SC} = SU(2)_C \otimes SU(2)_L \otimes SU(2)_R. \tag{3.2}$$

In the 2SC phase the flavor remains unbroken and the color gauge group is broken down to $SU(2)_C$. Two-flavor pairing is relevant at intermediate chemical potential μ where the strange quark mass can effectively be considered infinite, $m_s \to \infty$. In this phase, there is no chiral as well as global symmetry breaking. The color-flavor structure of the order parameter Δ in 2SC phase is given by [8]

$$\Phi_{ij}^{ab} = \epsilon^{ab3}\epsilon^{ij},$$

where i, j are flavor indices: $(i = 1, 2)$ and a, b are color indices: $(a = 1, 2, 3)$. ϵ^{ij} and ϵ^{ab3} are antisymmetric tensors in the flavor and color spaces, respectively. In the 2SC phase, there is also an unbroken $\tilde{U}(1)$ gauge symmetry. The corresponding generator reads [8]

$$\tilde{Q} = Q - \frac{T_8}{\sqrt{3}}. \tag{3.3}$$

As there is no breaking of $U(1)$ symmetry, the two-flavor quark matter is $\tilde{Q}$-neutral and the rotated photon does not acquire a Meissner mass. The quarks carry a rotated $\tilde{Q}$ charge. In units of $\tilde{e} = ecos\theta$, where for 2SC $cos\theta = \dfrac{g}{(\frac{e^2}{12} + g^2)^{\frac{1}{2}}}$ and e and g are the electromagnetic and coupling constants, these charges are [8]

$$\begin{aligned} \tilde{Q}(u_r) = \tilde{Q}(u_g) = +\frac{1}{2},\ \tilde{Q}(u_b) = 1 \\ \tilde{Q}(d_r) = \tilde{Q}(d_g) = -\frac{1}{2},\ \tilde{Q}(d_b) = 0. \end{aligned} \tag{3.4}$$

3.2.2 Three Flavor Color Superconductor

Now, we consider three massless quark flavors, $N_f = 3$. As in the 2SC phase, the condensation of Cooper pairs occurs in the antisymmetric flavor and spin channels, which, together with the antisymmetric color channel, ensures the antisymmetry of the pair wave function. But the difference is caused by different numbers of flavors which takes the antisymmetric flavor representation antitriplet unlike in 2SC phase where it is singlet. As a result, the color-flavor structure of the order parameter Δ in case of three-flavor color superconductor is

$$\Phi_{ij}^{ab} = \epsilon^{ab3}\epsilon^{ij3},$$

which corresponds to the so-called Color-Flavor-Locked (CFL) phase. Here i, j are flavor indices: $(i = 1, 2, 3)$ and a, b are color indices: $(a = 1, 2, 3)$. ϵ^{ij3} and ϵ^{ab3} are antisymmetric tensors in the flavor and color spaces, respectively. The CFL phase is the most favored phase at asymptotically large densities. In this phase, the order parameter Δ breaks chiral symmetry in the form

$$SU(3)_C \times SU(3)_L \times SU(3)_R \rightarrow SU(3)_{C+L+R}.$$

In this phase, the order parameter is invariant under joint rotations in color and flavor space. This, of course, is the reason for the term color-flavor locking. Furthermore, as in the 2SC phase, there is a local residual $U(1)$ originating from both the color and electromagnetic gauge groups.

3.3 Color Superconductivity in a Magnetic Field

Here we briefly discuss the underlying concepts of color superconductivity in the presence of a magnetic field. Secondly, we review some of the pertinent ideas and results of three flavor (CFL) in presence of a magnetic field previously made.

As we mentioned earlier, in conventional superconductivity, electron Cooper pairs form a charged condensate, thereby spontaneously breaking the $U(1)_{em}$ gauge symmetry of electromagnetism. Consequently, external magnetic fields are screened by photon of finite effective mass, the so-called Meissner effect. In spin-zero color superconductivity, unlike conventional superconductivity, the $U(1)_{em}$ symmetry is not broken, but merely rotated because the quark Cooper pairs are neutral with respect to a $\tilde{U}(1)$ symmetry [17]. This rotated symmetry, $\tilde{U}(1)_{em}$, has an associated charge $\tilde{Q}$, and field $\tilde{A}_\mu = A_\mu cos\theta - G^8_\mu sin\theta$. Here the angle of rotation, called mixing angle, is very small, implying that the rotated field is mainly comprised of the original photon with a small gluon admixture. Since the rotated photon is massless, a rotated magnetic field B therefore penetrates the color superconductor. Although the pairing occurs in such a way that it leaves the condensate $\tilde{Q}$-neutral, some of the individual quarks may carry a $\tilde{Q}$ charge in pairing. This implies that each component of pairs are either both neutral, or oppositely charged. The charged quarks in the pair can couple to an external magnetic field and this can significantly alter the gap structure and lead to a new superconducting phase. The effect of a magnetic field was studied in [18, 19] and a new phase called Magnetic Color -Flavor-Locked (MCFL) was discovered.

Why do we need to introduce magnetic field in color superconductivity? As we said earlier, in the highly-dense interior of neutron stars, the color superconducting state is expected to be found . It is also known that there exists a very large

magnetic field at the surface of these compact stars. For example, at ordinary neutron stars, the field strength at the surface can be of order $B \sim 10^{11} - 10^{13}$ G [20], while at magnetars fields may be as great as $B \sim 10^{14} - 10^{15}$ G [21]. By comparing the energy of magnetic and gravitational fields, the upper limit for the field strengths of gravitationally bound stars is set at $B \sim 10^{18} - 10^{19}$ G [22, 23]. This limit is even larger if quarks are self-bound [23]. It has been found that the energy scale set by such strong magnetic fields is of the order similar to that of the color superconducting gaps ($\Delta \sim 10 - 100$ MeV). Therefore, it is expected that large fields may in some way modify the structure of the gap. At this scenario, its inevitable to introduce the magnetic fields to understand the pairing patterns and magnitudes of the quark pair condensates. In our work we set to study the effects of a magnetic field on the 2SC phase. From this analysis we might get an understanding of the way color superconducting matter may realistically appear in observations of compact stars. Before discussing 2SC pairing in a magnetic field, we briefly review here what has been found for the three-flavor CFL pattern when a magnetic field is introduced. It has been shown that the CFL gap structure is modified when a magnetic field is present [19]. That work has been done within the framework of effective field theories to obtain the gap equations for arbitrary field values. In those studies, analytical calculations were also carried out in the large field limit as well as at zero field [19], to make sure that the pairing gaps match those originally found for CFL in the absence of a magnetic field. Also, numerical studies have been done in a range of relevant magnetic field which show that the color-flavor locked gaps [24, 25], chemical potentials [24], and magnetization [25] of the dense cold quark matter oscillate with the magnetic field.

3.4 CFL in a Magnetic Field

As we described in 3.2.2, the CFL gap structure breaks the $S(3)_C \times SU(3)_L \times SU(3)_R$ symmetry of QCD down to the diagonal group $SU(3)_{C+L+R}$, which locks color and flavor rotations. In addition, there remains a linear combination of the $8th$ color generator and the electromagnetic generator under which the condensate is invariant. This is the generator of the rotated $\tilde{U}(1)_{em}$ symmetry we have mentioned above.

The $\tilde{Q}$ charges of the quarks, in units of $\tilde{e} = e\cos\theta$, are as follows

s_b	s_g	s_r	d_b	d_g	d_r	u_b	u_g	u_r
0	0	-	0	0	-	+	+	0

where the subscripts (b, g, r) represent the colors of corresponding quarks. CFL matter in the presence of a strong rotated magnetic field was introduced in [18]. In the CFL matter with B, it was found that the gap structure is modified, leading to a new pattern, that of MCFL. Although MCFL involves three quark flavors with three colors like CFL, CFL and its magnetic counter parts differ in several ways: for instance MCFL has a lower symmetry, the full CFL group being reduced by the presence of a magnetic field. In case of unpaired quark matter with up, down, and strange quarks, the presence of a magnetic field already reduces the chiral symmetry-$SU(3)_L \times SU(3)_R \rightarrow SU(2)_L \times SU(2)_R$. If a color-breaking condensate is also considered, there is the further reduction, $SU(3)_C \times SU(2)_L \times SU(2)_R \rightarrow SU(2)_{C+L+R}$ giving rise to the symmetry characterizing MCFL. The structure of

the MCFL gap as described in [19] is

$$\Delta = \begin{pmatrix} 2\Delta_{S'} & 0 & 0 & \Delta_A+\Delta_S & 0 & 0 & 0 & 0 & \Delta_A^B+\Delta_S^B \\ 0 & 0 & 0 & \Delta_S-\Delta_A & 0 & 0 & 0 & 0 & 0 \\ 0 & 0 & 0 & 0 & 0 & 0 & \Delta_S^B-\Delta_A^B & 0 & 0 \\ 0 & \Delta_S-\Delta_A & 0 & 0 & 0 & 0 & 0 & 0 & 0 \\ \Delta_A+\Delta_S & 0 & 0 & 0 & 2\Delta_{S'} & 0 & 0 & 0 & \Delta_A^B+\Delta_S^B \\ 0 & 0 & 0 & 0 & 0 & 0 & 0 & \Delta_S^B-\Delta_A^B & 0 \\ 0 & 0 & \Delta_S^B-\Delta_A^B & 0 & 0 & 0 & 0 & 0 & 0 \\ 0 & 0 & 0 & 0 & 0 & \Delta_S^B-\Delta_A^B & 0 & 0 & 0 \\ \Delta_A^B+\Delta_S^B & 0 & 0 & 0 & \Delta_A^B+\Delta_S^B & 0 & 0 & 0 & 2\Delta_{S''} \end{pmatrix} . \quad (3.5)$$

Here the gaps Δ_A^B and Δ_S^B are antisymmetric and symmetric in their color-flavor structures. The superindex B indicates that these gaps get contributions from pairs of oppositely charged quarks and from pairs of neutral quarks. On the other hand, the antisymmetric Δ_A and symmetric Δ_S, $\Delta_{S'}$ and $\Delta_{S''}$ gaps only get contributions from pairs of neutral quarks. At zero field limit the gaps satisfy the conditions $\Delta_A = \Delta_A^B$ and $\Delta_S^B = \Delta_{S'} = \Delta_{S''}$, leaving only two CFL gaps as they should be.

As shown in [19] the presence of magnetic field strengthens the gap Δ_A^B. This could be explained intuitively by noting that these oppositely charged quarks also have opposite spins, and therefore have their magnetic moments aligned. This leads to a larger energy gap which results in a greater binding of pairs. Thus, unlike conventional superconductivity where the field-expelling Meissner effect is observed, MCFL color superconductivity is in fact favored by a strong external field. Physically, the increase in the gap at large magnetic fields is a direct result of the enhancement of the density of states at the Fermi surface of the charged quarks at the zero Landau level.

The expressions for the gaps characterizing the MCFL phase are derived in [19] in the context of an NJL model inspired by single-gluon exchange. Although these highly-coupled, non-linear gap equations can be solved only numerically,

they can also be solved analytically as well in very large and zero magnetic field. In the zero field limit, it is been found that MCFL gaps continuously transit to CFL gaps where the charged and neutral pairs of quarks are undistinguishable from each other. In this field limit, they found that $\Delta_A = \Delta_A^B >> \Delta_S = \Delta_S^B$ and the larger antisymmetric gap is given by

$$\Delta_A^{CFL} \sim 2\sqrt{\Lambda\mu - \mu^2}\exp\Big(-\frac{3\Lambda^2\pi^2}{2g^2\mu^2}\Big). \tag{3.6}$$

In the strong magnetic field regime, $\frac{2\tilde{e}\tilde{B}}{\mu^2} \geq 1$ assuming $\Delta_A^B >> \Delta_S^B, \Delta_A$ and $\Delta_A >> \Delta_S$, they found that

$$\Delta_A^B \sim 2\sqrt{\Lambda\mu - \mu^2}\exp\Big(-\frac{3\Lambda^2\pi^2}{g^2(\mu^2 + \frac{\tilde{e}\tilde{B}}{2})}\Big). \tag{3.7}$$

By looking at the expressions for the gaps at zero and large field we see that the gaps are similar to that of conventional BCS gap. At zero field the gap goes as $\exp\Big(-\frac{1}{N\tilde{G}}\Big)$ where $\tilde{G} = \frac{g^2}{3\pi^2}$ is a dimensionless coupling constant and N corresponds to the total density of states at the Fermi surface of those quarks contributing to the gap. Here the density of states for a single quark is $N_\mu = \frac{\mu^2}{2\pi^2}$, as there are four quarks involved in pairing the total density of states is $N = 4\tilde{N}$. In strong magnetic field, there are two types of quarks contributing to the gaps, charged and neutral one. As a consequence the resulting density of states are N_μ and $N_{\tilde{B}}$ for neutral and charge quarks respectively. The total density of states is therefore $N = 2N_\mu + 2N_{\tilde{B}}$, as two of four quarks are charged.

From Eq.3.7 we see that in the strong field limit, the gap increases as a function of magnetic fields. If we further go beyond $\frac{2\tilde{e}\tilde{B}}{\mu^2} \geq 1$ regime, comparing the Eq.3.6 and Eq.3.7, one can see that the MCFL gap surpasses the CFL, $\Delta_A^B > \Delta_A^{CFL}$.

From the results of Ref. [19], we see that the gap structure of color-flavor locked quark matter is modified in the presence of a magnetic field, as this field splits the CFL gaps in two different antisymmetric gaps. This changed gap structure leads to the new color superconducting pattern, MCFL. Moreover, for fields sufficiently large, the MCFL gap having contributions from charged quarks exceeds the zero field CFL limit.

Now let us discuss briefly the behavior of the MCFL gaps for the range of fields $0 < \tilde{e}\tilde{B} < \mu^2$. In Refs. [24, 25], the gap equations were studied numerically. These authors found that the MCFL gaps oscillate with $\frac{\tilde{e}\tilde{B}}{\mu^2}$ [24, 25]. The magnetization of the quark matter is shown to also display similar oscillating behavior [25]. The origin of this oscillating behavior is similar to that of the de Haas-van Alphen oscillations occurring in metals. These in fact follow from the oscillatory nature of the density of states at the Fermi surface, which is in turn brought on by the quantization of energy levels (Landau levels) connected with the orbital motion of charged particles due to field. As the magnetic field is increased, the Landau levels move farther from one another, passing through the Fermi surface, where the density of available states then varies. Since Cooper pairing takes place among those particles at the Fermi surface, a change in the occupation number there results in more or less pairing. When the temperature is lowered, many properties of a fermion system depend on the density of states at the Fermi surface. Any quantity depending on the density of states[25] shows a similar behavior. As we mentioned above, the gap explicitly depends on the quark density of states. In superconductivity, the gap behaves as the order parameter whose finite value marks the existence of the superconducting state(ordered phase). Therefore, there must be a connection between any other physical quantities associated with superconductivity and the gap. As a result of this chain of dependency,

these quantities also oscillate with the varying magnetic field. In Ref.[25], they have also neglected two symmetric channels, leaving only two gap parameters, one (denoted by Δ in [25]) formed from pairs of quarks with opposite rotated charge as well as pairs of neutral quarks, and the other (ϕ) having contributions only from pairs of neutral quarks. When at large magnetic fields, the authors find qualitative agreement with Ref.[19], showing that for very large fields, $\Delta > \phi$ in the same physical setting.

The work of Ref.[19] as well as of Ref.[25] were done without imposing charge neutrality. Also in Ref.[25] work, color chemical potentials were left out, as they are thought to be small for $\frac{\tilde{e}\tilde{B}}{\mu^2} \leq 1$. These two points together allow us to set the three chemical potentials for the up, down, and strange quarks to be equal.

The full consideration of electric and color neutrality in the MCFL setting were made in Ref.[24]. The conditions for neutrality were obtained by introducing electric and color chemical potentials, μ_e, μ_3, and μ_8 .

The gaps representing the predominant pairing between down and strange (d-s) quarks, strange and up (s-u) quarks, and up and down (u-d) quarks are Δ_1 , Δ_2, and Δ_3, respectively. As each of the three light quarks pair symmetrically in CFL phase, these gaps are equivalent to each other i.e., $\Delta_1 \sim \Delta_2 \sim \Delta_3$. In absence of neutrality condition, if a magnetic field is introduced, it is found [24] that $\Delta_2 \sim \Delta_3 \geq \Delta_1$ for $\frac{2\tilde{e}\tilde{B}}{\mu^2} > 1$. If the neutrality conditions are also imposed, magnitude of the gap changes significantly at very large fields, with $\Delta_1 >> \Delta_2 \sim \Delta_3$[24]. The authors point that this rearranging of the gaps follows from the way that the Fermi surface for each pairing is affected when neutrality is considered. One should remember that these results were obtained without considering the two symmetric gaps with respect to the antisymmetric gaps. This assumption may not be true for large fields, as Δ_S^B may rise with the field

and surpass Δ_A according to Ref.[19]. In Ref.[24] they have also studied the field dependence of chemical potential which is an oscillating function of field.

Chapter 4

2SC and Chromomagnetic Instability

In this chapter, we discuss the main part of our the thesis, that is two flavor color superconductivity in the presence of a magnetic field. For the sake of understanding we will briefly mention the instability that appears in the 2SC phase in some regions of the physical parameters. As we will see, our results signal the possibility to cure that instability with a strong enough magnetic field.

4.1 2SC in a Magnetic Field

As mentioned earlier, the 2SC phase is described by the simplest $SU(2)$ NJL model that was proposed in [26]. The explicit form of the Lagrangian density in the presence of a magnetic field is given by

$$L = \bar{q}\gamma^{\mu}(i\partial_{\mu} - \tilde{e}\tilde{A}_{\mu})q + G_D[(i\bar{q}^C\epsilon\epsilon^b\gamma_5 q)(i\bar{q}\epsilon\epsilon^b\gamma_5 q^C)] \tag{4.1}$$

where $\bar{q} = C\bar{q}^T$ is the charge-conjugate spinor and $C = i\gamma^2\gamma^0$ is the charge conjugation operator. The quark field $q \equiv q_{i\alpha}$ is a four-component Dirac spinor that carries flavor ($i = 1, 2$) and color ($\alpha = 1, 2, 3$) indices. ϵ^{ij} and $\epsilon^{\alpha\beta b}$ are antisymmetric tensors in the flavor and color spaces, respectively. $\tilde{A}_{\mu}$ is the vector

potential associated with the rotated magnetic field and $\tilde{e}$ is the rotated charge. In the mean-field approximation, at zero temperature, the effective thermodynamic potential at finite magnetic field derived from Lagrangian Eq.4.1 is given by

$$\begin{aligned}
\Omega = \Omega_0 + \frac{\Delta^2}{4G} - \frac{\mu_{db}^4}{12\pi^2} \\
-\frac{eB}{4\pi^2}\sum_{n=0}^{\frac{\mu_e^2}{2eB}}(2-\delta_{n0})\big[\frac{\mu_e}{2}\sqrt{\mu_e^2-2eBn} - eBn\ln(\frac{\sqrt{\mu_e^2-2eBn}+\mu_e}{\sqrt{2eBn}})\big] \\
-\frac{eB}{4\pi^2}\sum_{n=0}^{\frac{\mu_{ub}^2}{2eB}}(2-\delta_{n0})\big[\frac{\mu_{ub}}{2}\sqrt{\mu_{ub}^2-2eBn} - eBn\ln(\frac{\sqrt{\mu_{ub}^2-2eBn}+\mu_{ub}}{\sqrt{2eBn}})\big] \\
-\frac{eB}{\pi^2}\sum_{n=0}^{\infty}(1-\frac{\delta_{n0}}{2})\int_0^{\infty} e^{-\frac{(p_3^2+eBn)}{\lambda^2}}\big(\sqrt{(\sqrt{p_3^2+eBn}+\bar{\mu})^2+\Delta^2}\big)dp_3 \\
-\frac{eB}{2\pi^2}\sum_{n=0}^{\infty}(1-\frac{\delta_{n0}}{2})\int_0^{\infty} e^{-\frac{(p_3^2+eBn)}{\lambda^2}}\big(|\sqrt{(\sqrt{p_3^2+eBn}-\bar{\mu})^2+\Delta^2}+\delta\mu|\big)dp_3 \\
-\frac{eB}{2\pi^2}\sum_{n=0}^{\infty}(1-\frac{\delta_{n0}}{2})\int_0^{\infty} e^{-\frac{(p_3^2+eBn)}{\lambda^2}}\big(|\sqrt{(\sqrt{p_3^2+eBn}-\bar{\mu})^2+\Delta^2}-\delta\mu|\big)dp_3. \quad (4.2)
\end{aligned}$$

Where the coupling constant is $G \equiv \eta G_s$, η is positive and of order one, and $G_S = 5.0163$ GeV^2. Here η should be positive which implies that there is an attraction in the color- antisymmetric channel, as is suggested by first-principle QCD calculations [6, 16]. Here, e denotes the rotated charge which couples to the rotated magnetic field B; i.e., here we are using the notation $\tilde{e} \equiv e$ and $\tilde{B} \equiv B$. Δ denotes the gap parameter. At sufficiently large densities, the constituent masses of the pairing quarks can be neglected, and so no mass terms appear. The diagonal matrix of chemical potential as obtained from [27].

$$\mu_{ij,\alpha\beta} = (\mu\delta_{ij} - \mu_e Q_{ij})\delta_{\alpha\beta} + \frac{2}{\sqrt{3}}\mu_8\delta_{ij}(T_8)_{\alpha\beta} \quad (4.3)$$

where μ, μ_e and μ_8 are quark, electron and color chemical potentials and Q and T are generators of electromagnetic group $U(1)_{em}$ and the color subgroup $U(1)_8$ respectively. The chemical potential of each quark is as follows:

$$\mu_{ur} = \mu_{ug} = \mu - \frac{2}{3}\mu_e + \frac{1}{3}\mu_8 \tag{4.4}$$

$$\mu_{dr} = \mu_{dg} = \mu + \frac{1}{3}\mu_e + \frac{1}{3}\mu_8 \tag{4.5}$$

$$\mu_{db} = \mu + \frac{1}{3}\mu_e - \frac{2}{3}\mu_8 \tag{4.6}$$

$$\mu_{ub} = \mu - \frac{2}{3}\mu_e - \frac{2}{3}\mu_8. \tag{4.7}$$

As the 2SC quark matter is invariant under the $SU(2)_C$ color subgroup, we do not need to introduce a second color chemical potential μ_3 [27]. Based upon the notations of Ref. [27], we introduce the following entities as

$$\bar{\mu} \equiv \frac{\mu_{ur} + \mu_{dg}}{2} = \frac{\mu_{ug} + \mu_{dr}}{2} = \mu - \frac{\mu_e}{6} + \frac{\mu_8}{3} \tag{4.8}$$

and

$$\delta\mu \equiv \frac{\mu_{dg} - \mu_{ur}}{2} = \frac{\mu_{dr} - \mu_{ug}}{2} = \frac{\mu_e}{2} \tag{4.9}$$

where the last one is the mismatch parameter. Now let us simplify the Eq.4.2. For that, we can write the absolute values of the dispersions as

$$\begin{aligned}|\sqrt{(\sqrt{p_3^2 + eBn} - \bar{\mu})^2 + \Delta^2} - \delta\mu| = (\sqrt{(\sqrt{p_3^2 + eBn} - \bar{\mu})^2 + \Delta^2} - \delta\mu) \times \\ \Big[\theta(\sqrt{(\sqrt{p_3^2 + eBn} - \bar{\mu})^2 + \Delta^2} - \delta\mu) - \\ \theta(-(\sqrt{(\sqrt{p_3^2 + eBn} - \bar{\mu})^2 + \Delta^2} - \delta\mu))\Big].\end{aligned} \tag{4.10}$$

Using the identity

$$\theta(-(\sqrt{(\sqrt{p_3^2+eBn}-\bar{\mu})^2+\Delta^2}-\delta\mu))=1-\theta(\sqrt{(\sqrt{p_3^2+eBn}-\bar{\mu})^2+\Delta^2}-\delta\mu),$$

we get

$$|\sqrt{(\sqrt{p_3^2+eBn}-\bar{\mu})^2+\Delta^2}-\delta\mu|=(\sqrt{(\sqrt{p_3^2+eBn}-\bar{\mu})^2+\Delta^2}-\delta\mu)\times \Big[2\theta(\sqrt{(\sqrt{p_3^2+eBn}-\bar{\mu})^2+\Delta^2}-\delta\mu)-1\Big]. \quad (4.11)$$

Case I: If $\Delta > \delta\mu$, then

$$\theta(\sqrt{(\sqrt{p_3^2+eBn}-\bar{\mu})^2+\Delta^2}-\delta\mu)=1.$$

Case II: If $\delta\mu > \Delta$, we have to analyze the regions for the θ function. Let us find the solutions of argument of θ. We can easily figure out that

$$\sqrt{(\sqrt{p_3^2+eBn}-\bar{\mu})^2+\Delta^2}-\delta\mu=0$$

will have two solutions: $p_1=\sqrt{(\bar{\mu}-\sqrt{\delta\mu^2-\Delta^2})^2-eBn}$ and

$$p_2=\sqrt{(\bar{\mu}+\sqrt{\delta\mu^2-\Delta^2})^2-eBn}.$$

So we have $\theta(f(p_3))=1$, where $f(p_3)=\Big(\sqrt{(\sqrt{p_3^2+eBn}-\bar{\mu})^2+\Delta^2}-\delta\mu\Big)$, for $p_3 \leq p_1$ and $\geq p_2$. Since the momenta p cannot be imaginary, the corresponding sums over Landau level can be extended only up to

$$n_1=\frac{(\bar{\mu}-\sqrt{\delta\mu^2-\Delta^2})^2}{eB}$$

and

$$n_2 = \frac{(\bar{\mu} + \sqrt{\delta\mu^2 - \Delta^2})^2}{eB}$$

for the regions $p \leq p_1$ and $p \geq p_2$, respectively. To investigate whether the θ function has a contribution or not in the region between p_1 and p_2, we need to know the behavior(value) of the argument of the θ function. Let us minimize the argument of the θ function with respect to p_3, we have

$$\frac{d\sqrt{(\sqrt{p_3^2 + eBn} - \bar{\mu})^2 + \Delta^2} - \delta\mu}{dp_3} = 0$$
$$= \frac{p_3(\sqrt{p_3^2 + eBn} - \bar{\mu})}{(\sqrt{p_3^2 + eBn})\sqrt{(\sqrt{p_3^2 + eBn} - \bar{\mu})^2 + \Delta^2}}.$$

Therefore we have two stationary solutions: the zero value which corresponds to the trivial non-physical solution and the other one which depends on the Landau level n, baryonic chemical potential μ and the magnetic field B

$$p_3 = 0 \quad or \quad \sqrt{(\bar{\mu}^2 - eBn)}.$$

Again differentiating with respect to p_3 we get,

$$\frac{d^2\sqrt{(\sqrt{p_3^2 + eBn} - \bar{\mu})^2 + \Delta^2} - \delta\mu}{dp_3^2}$$
$$= \Big[\frac{\sqrt{p_3^2 + eBn}\sqrt{(\sqrt{p_3^2 + eBn} - \bar{\mu})^2 + \Delta^2}\Big[(\sqrt{p_3^2 + eBn} - \bar{\mu}) + \frac{p_3^2}{\sqrt{p_3^2 + eBn}}\Big]}{\Big[\sqrt{p_3^2 + eBn}\sqrt{(\sqrt{p_3^2 + eBn} - \bar{\mu})^2 + \Delta^2}\Big]^2}$$
$$- \frac{p_3(\sqrt{p_3^2 + eBn} - \bar{\mu})d\Big[\sqrt{p_3^2 + eBn}\sqrt{(\sqrt{p_3^2 + eBn} - \bar{\mu})^2 + \Delta^2}\Big]/dp_3}{\Big[\sqrt{p_3^2 + eBn}\sqrt{(\sqrt{p_3^2 + eBn} - \bar{\mu})^2 + \Delta^2}\Big]^2}\Big]. \quad (4.12)$$

At $p_3 = \sqrt{(\bar{\mu}^2 - eBn)}$ the first and last term vanishes, therefore

$$\frac{d^2\sqrt{(\sqrt{p_3^2+eBn}-\bar{\mu})^2+\Delta^2}-\delta\mu}{dp_3^2} = \frac{p_3^2}{(\sqrt{p_3^2+eBn})\sqrt{(\sqrt{p_3^2+eBn}-\bar{\mu})^2+\Delta^2}} > 0.$$

So the function $f(p_3)$ has a minimum which lies between p_1 and p_2. On the other hand, we get $\theta(-f(p_3)) = 1$ for $p_1 \leq p \leq p_2$. The sum over Landau level can extend maximum up to n_1. Now the last integral can be rewritten as

$$\begin{aligned} I_1 = \frac{eB}{\pi^2}\Big[&\sum_{n=0}^{\infty}(1-\frac{\delta_{n0}}{2})\theta(\Delta-\delta\mu)\int_0^{\infty} e^{-}\frac{(p_3^2+eBn)}{\lambda^2}f(p_3)dp_3 \\ &+\sum_{n=0}^{n_1}(1-\frac{\delta_{n0}}{2})\theta(\delta\mu-\Delta)\int_0^{p_1} e^{-}\frac{(p_3^2+eBn)}{\lambda^2}f(p_3)dp_3 \\ &+\sum_{n=0}^{n_2}(1-\frac{\delta_{n0}}{2})\theta(\delta\mu-\Delta)\int_{p_2}^{\infty} e^{-}\frac{(p_3^2+eBn)}{\lambda^2}f(p_3)dp_3 \\ &-\frac{1}{2}\sum_{n=0}^{\infty}(1-\frac{\delta_{n0}}{2})\int_0^{\infty} e^{-}\frac{(p_3^2+eBn)}{\lambda^2}f(p_3)dp_3\Big]. \end{aligned}$$

Again using the relation

$$\theta(\Delta-\delta\mu) = 1-\theta(\delta\mu-\Delta),$$

we obtain

$$\begin{aligned} I_1 = \frac{eB}{2\pi^2}\Big[&2\sum_{n=0}^{\infty}(1-\frac{\delta_{n0}}{2})\int_0^{\infty} e^{-}\frac{(p_3^2+eBn)}{\lambda^2}f(p_3)dp_3 \\ -2&\sum_{n=0}^{\infty}(1-\frac{\delta_{n0}}{2})\theta(\delta\mu-\Delta)\int_0^{\infty} e^{-}\frac{(p_3^2+eBn)}{\lambda^2}f(p_3)dp_3 \\ +2&\sum_{n=0}^{n_1}(1-\frac{\delta_{n0}}{2})\theta(\delta\mu-\Delta)\int_0^{p_1} e^{-}\frac{(p_3^2+eBn)}{\lambda^2}f(p_3)dp_3 \end{aligned}$$

$$+2\sum_{n=0}^{n_2}(1-\frac{\delta_{n0}}{2})\theta(\delta\mu-\Delta)\int_{p_2}^{\infty}e^{-}\frac{(p_3^2+eBn)}{\lambda^2}f(p_3)dp_3$$
$$-\sum_{n=0}^{\infty}(1-\frac{\delta_{n0}}{2})\int_{0}^{\infty}e^{-}\frac{(p_3^2+eBn)}{\lambda^2}f(p_3)dp_3\Big].$$

Splitting the sum $\sum_{n=0}^{\infty}=\sum_{n=0}^{n_2}+\sum_{n=n_2+1}^{\infty}$ and the integral $\int_0^{\infty}=\int_0^{p_2}+\int_{p_2}^{\infty}$

$$I_1=\frac{eB}{2\pi^2}\Big[\sum_{n=0}^{\infty}(1-\frac{\delta_{n0}}{2})\int_0^{\infty}e^{-}\frac{(p_3^2+eBn)}{\lambda^2}\big(\sqrt{(\sqrt{p_3^2+eBn}-\bar{\mu})^2+\Delta^2}-\delta\mu\big)dp_3$$
$$-2\sum_{n=0}^{n_2}(1-\frac{\delta_{n0}}{2})\theta(\delta\mu-\Delta)\int_0^{p_2}e^{-}\frac{(p_3^2+eBn)}{\lambda^2}\big(\sqrt{(\sqrt{p_3^2+eBn}-\bar{\mu})^2+\Delta^2}-\delta\mu\big)dp_3$$
$$-2\sum_{n=0}^{n_2}(1-\frac{\delta_{n0}}{2})\theta(\delta\mu-\Delta)\int_{p_2}^{\infty}e^{-}\frac{(p_3^2+eBn)}{\lambda^2}\big(\sqrt{(\sqrt{p_3^2+eBn}-\bar{\mu})^2+\Delta^2}-\delta\mu\big)dp_3$$
$$-2\sum_{n=n_2+1}^{\infty}(1-\frac{\delta_{n0}}{2})\theta(\delta\mu-\Delta)\int_0^{\infty}e^{-}\frac{(p_3^2+eBn)}{\lambda^2}\big(\sqrt{(\sqrt{p_3^2+eBn}-\bar{\mu})^2+\Delta^2}-\delta\mu\big)dp_3$$
$$+2\sum_{n=0}^{n_1}(1-\frac{\delta_{n0}}{2})\theta(\delta\mu-\Delta)\int_0^{p_1}e^{-}\frac{(p_3^2+eBn)}{\lambda^2}\big(\sqrt{(\sqrt{p_3^2+eBn}-\bar{\mu})^2+\Delta^2}-\delta\mu\big)dp_3$$
$$+2\sum_{n=0}^{n_2}(1-\frac{\delta_{n0}}{2})\theta(\delta\mu-\Delta)\int_{p_2}^{\infty}e^{-}\frac{(p_3^2+eBn)}{\lambda^2}\big(\sqrt{(\sqrt{p_3^2+eBn}-\bar{\mu})^2+\Delta^2}-\delta\mu\big)dp_3\Big].$$

Similarly, $\sum_{n=0}^{n_2}=\sum_{n=0}^{n_1}+\sum_{n=n_1+1}^{n_2}$ and $\int_0^{p_2}=\int_0^{p_1}+\int_{p_1}^{p_2}$, we get

$$I_1=\frac{eB}{2\pi^2}\Big[\sum_{n=0}^{\infty}(1-\frac{\delta_{n0}}{2})\int_0^{\infty}e^{-}\frac{(p_3^2+eBn)}{\lambda^2}\big(\sqrt{(\sqrt{p_3^2+eBn}-\bar{\mu})^2+\Delta^2}-\delta\mu\big)dp_3$$
$$-2\sum_{n=0}^{n_1}(1-\frac{\delta_{n0}}{2})\theta(\delta\mu-\Delta)\int_0^{p_1}e^{-}\frac{(p_3^2+eBn)}{\lambda^2}\big(\sqrt{(\sqrt{p_3^2+eBn}-\bar{\mu})^2+\Delta^2}-\delta\mu\big)dp_3$$
$$-2\sum_{n=0}^{n_1}(1-\frac{\delta_{n0}}{2})\theta(\delta\mu-\Delta)\int_{p_1}^{p_2}e^{-}\frac{(p_3^2+eBn)}{\lambda^2}\big(\sqrt{(\sqrt{p_3^2+eBn}-\bar{\mu})^2+\Delta^2}-\delta\mu\big)dp_3$$
$$-2\sum_{n=n_1+1}^{n_2}(1-\frac{\delta_{n0}}{2})\theta(\delta\mu-\Delta)\int_0^{p_2}e^{-}\frac{(p_3^2+eBn)}{\lambda^2}\big(\sqrt{(\sqrt{p_3^2+eBn}-\bar{\mu})^2+\Delta^2}-\delta\mu\big)dp_3$$

$$-2\sum_{n=n_2+1}^{\infty}(1-\frac{\delta_{n0}}{2})\theta(\delta\mu-\Delta)\int_0^{\infty}e^{-}\frac{(p_3^2+eBn)}{\lambda^2}\big(\sqrt{(\sqrt{p_3^2+eBn}-\bar{\mu})^2+\Delta^2}-\delta\mu\big)dp_3$$
$$+2\sum_{n=0}^{n_1}(1-\frac{\delta_{n0}}{2})\theta(\delta\mu-\Delta)\int_0^{p_1}e^{-}\frac{(p_3^2+eBn)}{\lambda^2}\big(\sqrt{(\sqrt{p_3^2+eBn}-\bar{\mu})^2+\Delta^2}-\delta\mu\big)dp_3\Big].$$

Hence, after simplification we get

$$I_1=\frac{eB}{2\pi^2}\Big[\sum_{n=0}^{\infty}(1-\frac{\delta_{n0}}{2})\int_0^{\infty}e^{-}\frac{(p_3^2+eBn)}{\lambda^2}\big(\sqrt{(\sqrt{p_3^2+eBn}-\bar{\mu})^2+\Delta^2}-\delta\mu\big)dp_3$$
$$-\theta(\delta\mu-\Delta)\Big[2\sum_{n=0}^{n_1}(1-\frac{\delta_{n0}}{2})\int_{p_1}^{p_2}e^{-}\frac{(p_3^2+eBn)}{\lambda^2}\big(\sqrt{(\sqrt{p_3^2+eBn}-\bar{\mu})^2+\Delta^2}-\delta\mu\big)dp_3$$
$$+2\sum_{n=n_1+1}^{n_2}(1-\frac{\delta_{n0}}{2})\int_0^{p_2}e^{-}\frac{(p_3^2+eBn)}{\lambda^2}\big(\sqrt{(\sqrt{p_3^2+eBn}-\bar{\mu})^2+\Delta^2}-\delta\mu\big)dp_3$$
$$+2\sum_{n=n_2+1}^{\infty}(1-\frac{\delta_{n0}}{2})\int_0^{\infty}e^{-}\frac{(p_3^2+eBn)}{\lambda^2}\big(\sqrt{(\sqrt{p_3^2+eBn}-\bar{\mu})^2+\Delta^2}-\delta\mu\big)dp_3\Big]\Big].$$

Substituting I_1 back to the original equation we get,

$$\Omega=\Omega_0+\frac{\Delta^2}{4G}-\frac{\mu_{db}^4}{12\pi^2}$$
$$-\frac{eB}{4\pi^2}\sum_{n=0}^{\frac{\mu_e^2}{2eB}}(2-\delta_{n0})\big[\frac{\mu_e}{2}\sqrt{\mu_e^2-2eBn}-eBn\ln(\frac{\sqrt{\mu_e^2-2eBn}+\mu_e}{\sqrt{2eBn}})\big]$$
$$-\frac{eB}{4\pi^2}\sum_{n=0}^{\frac{\mu_{ub}^2}{2eB}}(2-\delta_{n0})\big[\frac{\mu_{ub}}{2}\sqrt{\mu_{ub}^2-2eBn}-eBn\ln(\frac{\sqrt{\mu_{ub}^2-2eBn}+\mu_{ub}}{\sqrt{2eBn}})\big]$$
$$-\frac{eB}{\pi^2}\sum_{n=0}^{\infty}(1-\frac{\delta_{n0}}{2})\int_0^{\infty}e^{-}\frac{(p_3^2+eBn)}{\lambda^2}\big(\sqrt{(\sqrt{p_3^2+eBn}+\bar{\mu})^2+\Delta^2}\big)dp_3$$
$$-\frac{eB}{2\pi^2}\sum_{n=0}^{\infty}(1-\frac{\delta_{n0}}{2})\int_0^{\infty}e^{-}\frac{(p_3^2+eBn)}{\lambda^2}\big(\sqrt{(\sqrt{p_3^2+eBn}-\bar{\mu})^2+\Delta^2}+\delta\mu\big)dp_3$$
$$-\frac{eB}{2\pi^2}\sum_{n=0}^{\infty}(1-\frac{\delta_{n0}}{2}\int_0^{\infty}e^{-}\frac{(p_3^2+eBn)}{\lambda^2}\big(\sqrt{(\sqrt{p_3^2+eBn}-\bar{\mu})^2+\Delta^2}-\delta\mu\big)dp_3+\frac{eB}{\pi^2}\times$$
$$\theta(\delta\mu-\Delta)\Big[\sum_{n=0}^{n_1}(1-\frac{\delta_{n0}}{2})\int_{p_1}^{p_2}e^{-}\frac{(p_3^2+eBn)}{\lambda^2}\big(\sqrt{(\sqrt{p_3^2+eBn}-\bar{\mu})^2+\Delta^2}-\delta\mu\big)dp_3$$

$$+\sum_{n=n_1+1}^{n_2}(1-\frac{\delta_{n0}}{2})\int_0^{p_2}e^{-}\frac{(p_3^2+eBn)}{\lambda^2}\Big(\sqrt{(\sqrt{p_3^2+eBn}-\bar{\mu})^2+\Delta^2}-\delta\mu\Big)dp_3$$
$$+\sum_{n=n_2+1}^{\infty}(1-\frac{\delta_{n0}}{2})\int_0^{\infty}e^{-}\frac{(p_3^2+eBn)}{\lambda^2}\Big(\sqrt{(\sqrt{p_3^2+eBn}-\bar{\mu})^2+\Delta^2}-\delta\mu\Big)dp_3\Big].$$

Again rearranging the terms, we obtain

$$\begin{aligned}\Omega=\Omega_0+\frac{\Delta^2}{4G}-\frac{\mu_{db}^4}{12\pi^2}\\
-\frac{eB}{4\pi^2}\sum_{n=0}^{\frac{\mu_e^2}{2eB}}(2-\delta_{n0})\big[\frac{\mu_e}{2}\sqrt{\mu_e^2-2eBn}-eBn\ln(\frac{\sqrt{\mu_e^2-2eBn}+\mu_e}{\sqrt{2eBn}})\big]\\
-\frac{eB}{4\pi^2}\sum_{n=0}^{\frac{\mu_{ub}^2}{2eB}}(2-\delta_{n0})\big[\frac{\mu_{ub}}{2}\sqrt{\mu_{ub}^2-2eBn}-eBn\ln(\frac{\sqrt{\mu_{ub}^2-2eBn}+\mu_{ub}}{\sqrt{2eBn}})\big]\\
-\frac{eB}{\pi^2}\sum_{n=0}^{\infty}(1-\frac{\delta_{n0}}{2})\int_0^{\infty}e^{-}\frac{(p_3^2+eBn)}{\lambda^2}\Big(\sqrt{(\sqrt{p_3^2+eBn}+\bar{\mu})^2+\Delta^2}\Big)dp_3\\
-\frac{eB}{\pi^2}\sum_{n=0}^{\infty}(1-\frac{\delta_{n0}}{2})\int_0^{\infty}e^{-}\frac{(p_3^2+eBn)}{\lambda^2}\Big(\sqrt{(\sqrt{p_3^2+eBn}-\bar{\mu})^2+\Delta^2}\Big)dp_3+\frac{eB}{\pi^2}\times\\
\theta(\delta\mu-\Delta)\Big[\sum_{n=0}^{n_1}(1-\frac{\delta_{n0}}{2})\int_{p_1}^{p_2}e^{-}\frac{(p_3^2+eBn)}{\lambda^2}\Big(\sqrt{(\sqrt{p_3^2+eBn}-\bar{\mu})^2+\Delta^2}-\delta\mu\Big)dp_3\\
+\sum_{n=n_1+1}^{n_2}(1-\frac{\delta_{n0}}{2})\int_0^{p_2}e^{-}\frac{(p_3^2+eBn)}{\lambda^2}\Big(\sqrt{(\sqrt{p_3^2+eBn}-\bar{\mu})^2+\Delta^2}-\delta\mu\Big)dp_3\\
+\sum_{n=n_2+1}^{\infty}(1-\frac{\delta_{n0}}{2})\int_0^{\infty}e^{-}\frac{(p_3^2+eBn)}{\lambda^2}\Big(\sqrt{(\sqrt{p_3^2+eBn}-\bar{\mu})^2+\Delta^2}-\delta\mu\Big)dp_3\Big].\end{aligned}\tag{4.13}$$

Gap Equation

Taking to the derivative of Ω in Eq.4.2 with respect to Δ, we get

$$\frac{\partial\Omega}{\partial\Delta}=0$$

$$\frac{\Delta}{2G} - \frac{eB}{\pi^2}\sum_{n=0}^{\infty}(1-\frac{\delta_{n0}}{2})\int_0^{\infty} e^{-}\frac{(p_3^2+eBn)}{\lambda^2}\Big[\frac{\Delta}{\sqrt{(\sqrt{p_3^2+eBn}+\bar{\mu})^2+\Delta^2}} + \frac{\Delta}{2\sqrt{(\sqrt{p_3^2+eBn}-\bar{\mu})^2+\Delta^2}}\Big]dp_3$$
$$-\frac{eB}{2\pi^2}\sum_{n=0}^{\infty}(1-\frac{\delta_{n0}}{2})\int_0^{\infty} e^{-}\frac{(p_3^2+eBn)}{\lambda^2}\frac{\partial|\sqrt{(\sqrt{p_3^2+eBn}-\bar{\mu})^2+\Delta^2}-\delta\mu|}{\partial\Delta} = 0. \tag{4.14}$$

Let us first rewrite the term I_1

$$I_1 = |\sqrt{(\sqrt{p_3^2+eBn}-\bar{\mu})^2+\Delta^2}-\delta\mu| = (\sqrt{(\sqrt{p_3^2+eBn}-\bar{\mu})^2+\Delta^2}-\delta\mu)\times \Big[2\theta(\sqrt{(\sqrt{p_3^2+eBn}-\bar{\mu})^2+\Delta^2}-\delta\mu)-1\Big]. \tag{4.15}$$

Differentiating w r to Δ,

$$I_2 = \frac{\partial|\sqrt{(\sqrt{p_3^2+eBn}-\bar{\mu})^2+\Delta^2}-\delta\mu|}{\partial\Delta} = \frac{\partial(\sqrt{(\sqrt{p_3^2+eBn}-\bar{\mu})^2+\Delta^2}-\delta\mu)}{\partial\Delta}$$
$$\Big[2\theta(\sqrt{(\sqrt{p_3^2+eBn}-\bar{\mu})^2+\Delta^2}-\delta\mu)-1\Big] + (\sqrt{(\sqrt{p_3^2+eBn}-\bar{\mu})^2+\Delta^2}-\delta\mu) \Big[2\frac{\partial\theta(\sqrt{(\sqrt{p_3^2+eBn}-\bar{\mu})^2+\Delta^2}-\delta\mu)}{\partial\Delta}\Big].$$

Let us take the second term

$$2(\sqrt{(\sqrt{p_3^2+eBn}-\bar{\mu})^2+\Delta^2}-\delta\mu)\Big[\frac{\partial\theta(\sqrt{(\sqrt{p_3^2+eBn}-\bar{\mu})^2+\Delta^2}-\delta\mu)}{\partial\Delta}\Big]$$
$$= 2(\sqrt{(\sqrt{p_3^2+eBn}-\bar{\mu})^2+\Delta^2}-\delta\mu) \Big[\delta(\sqrt{(\sqrt{p_3^2+eBn}-\bar{\mu})^2+\Delta^2}-\delta\mu)\frac{\Delta}{(\sqrt{(\sqrt{p_3^2+eBn}-\bar{\mu})^2+\Delta^2})}\Big].$$

Clearly, the integral

$$2\int_0^\infty \exp-\frac{(p_3^2+eBn)}{\Lambda^2}\sqrt{(\sqrt{p_3^2+eBn}-\bar{\mu})^2+\Delta^2}-\delta\mu)$$
$$\Big[\delta(\sqrt{(\sqrt{p_3^2+eBn}-\bar{\mu})^2+\Delta^2}-\delta\mu)\frac{\Delta}{(\sqrt{(\sqrt{p_3^2+eBn}-\bar{\mu})^2+\Delta^2})}\Big]dp_3=0.$$

Thanks to the delta function, the gap equation reduces to

$$\begin{aligned}\frac{\Delta}{2G}-\frac{eB}{\pi^2}\sum_{n=0}^{\infty}(1-\frac{\delta_{n0}}{2})\int_0^\infty e^-\frac{(p_3^2+eBn)}{\lambda^2}\Big[\frac{\Delta}{\sqrt{(\sqrt{p_3^2+eBn}+\bar{\mu})^2+\Delta^2}}\\ +\frac{\Delta}{2\sqrt{(\sqrt{p_3^2+eBn}-\bar{\mu})^2+\Delta^2}}\Big]dp_3\\ -\frac{eB}{2\pi^2}\sum_{n=0}^{\infty}(1-\frac{\delta_{n0}}{2})\int_0^\infty e^-\frac{(p_3^2+eBn)}{\lambda^2}\frac{\partial(\sqrt{(\sqrt{p_3^2+eBn}-\bar{\mu})^2+\Delta^2}-\delta\mu)}{\partial\Delta}\\ \Big[2\theta(\sqrt{(\sqrt{p_3^2+eBn}-\bar{\mu})^2+\Delta^2}-\delta\mu)-1\Big]=0.\end{aligned}\tag{4.16}$$

Using the same analogy that we use in simplifying potential we can rewrite the gap equation in the following form:

$$\begin{aligned}\frac{\Delta}{2G}-\frac{eB\Delta}{\pi^2}\sum_{n=0}^{\infty}(1-\frac{\delta_{n0}}{2})\int_0^\infty e^-\frac{(p_3^2+eBn)}{\lambda^2}\Big[\frac{1}{\sqrt{(\sqrt{p_3^2+eBn}+\bar{\mu})^2+\Delta^2}}\\ +\frac{1}{\sqrt{(\sqrt{p_3^2+eBn}-\bar{\mu})^2+\Delta^2}}\Big]dp_3\\ +\theta(\delta\mu-\Delta)\frac{eB\Delta}{\pi^2}\Big[\sum_{n=n_2+1}^{\infty}(1-\frac{\delta_{n0}}{2})\int_0^\infty\frac{e^-\frac{(p_3^2+eBn)}{\lambda^2}}{\sqrt{(\sqrt{p_3^2+eBn}-\bar{\mu})^2+\Delta^2}}\\ +\sum_{n=n_1+1}^{n_2}(1-\frac{\delta_{n_0}}{2})\int_{p_2}^\infty\frac{e^-\frac{(p_3^2+eBn)}{\lambda^2}}{\sqrt{(\sqrt{p_3^2+eBn}-\bar{\mu})^2+\Delta^2}}\end{aligned}$$

$$+\sum_{n=0}^{n_1}(1-\frac{\delta_{n0}}{2})\int_{p_1}^{p_2}\frac{e^{-\frac{(p_3^2+eBn)}{\lambda^2}}}{\sqrt{(\sqrt{p_3^2+eBn}-\bar{\mu})^2+\Delta^2}}\Big]dp_3$$
$$=0. \tag{4.17}$$

Electric Neutrality Equation

The electric neutrality condition is

$$\frac{\partial\Omega}{\partial\mu_e}=0. \tag{4.18}$$

Taking the derivatives of each term in Eq.4.2, we have

$$\frac{\partial\mu_{db}}{\partial\mu_e}=\frac{1}{3},$$

and

$$\frac{\partial\big[\frac{\mu_e}{2}\sqrt{\mu_e^2-2eBn}-eBn\ln(\frac{\sqrt{\mu_e^2-2eBn}+\mu_e}{\sqrt{2eBn}})\big]}{\partial\mu_e}$$
$$=\big[\frac{1}{2}\sqrt{\mu_e^2-2eBn}+\frac{\mu_e^2}{2\sqrt{\mu_e^2-2eBn}}$$
$$-eBn\frac{(1+\frac{\mu_e}{\sqrt{\mu_e^2-2eBn}})}{\sqrt{\mu_e^2-2eBn}+\mu_e}\big]$$
$$=\sqrt{\mu_e^2-2eBn}. \tag{4.19}$$

Similarly,

$$\frac{\partial\big[\frac{\mu_{ub}}{2}\sqrt{\mu_{ub}^2-2eBn}-eBn\ln(\frac{\sqrt{\mu_{ub}^2-2eBn}+\mu_{ub}}{\sqrt{2eBn}})\big]}{\partial\mu_e}$$
$$=\frac{-2}{3}\big[\frac{1}{2}\sqrt{\mu_{ub}^2-2eBn}+\frac{\mu_{ub}^2}{2\sqrt{\mu_{ub}^2-2eBn}}$$

$$-eBn\frac{(1+\frac{\mu_{ub}}{\sqrt{\mu_{ub}^2-2eBn}})}{\sqrt{\mu_{ub}^2-2eBn}+\mu_{ub}}\Big]$$
$$=\frac{-2}{3}\sqrt{\mu_{ub}^2-2eBn}. \tag{4.20}$$

Let us take the partial derivative of last term with respect to μ_e

$$\frac{\partial|\sqrt{(\sqrt{p_3^2+eBn}-\bar{\mu})^2+\Delta^2}-\delta\mu|}{\partial\mu_e}=\frac{2\partial(\sqrt{(\sqrt{p_3^2+eBn}-\bar{\mu})^2+\Delta^2}-\delta\mu)}{\partial\mu_e}$$
$$\Big[\theta(\sqrt{(\sqrt{p_3^2+eBn}-\bar{\mu})^2+\Delta^2}-\delta\mu)\Big]$$
$$+2(\sqrt{(\sqrt{p_3^2+eBn}-\bar{\mu})^2+\Delta^2}-\delta\mu)\Big[\frac{\partial\theta(\sqrt{(\sqrt{p_3^2+eBn}-\bar{\mu})^2+\Delta^2}-\delta\mu)}{\partial\mu_e}\Big].$$

Taking the second term

$$2(\sqrt{(\sqrt{p_3^2+eBn}-\bar{\mu})^2+\Delta^2}-\delta\mu)\Big[\frac{\partial\theta(\sqrt{(\sqrt{p_3^2+eBn}-\bar{\mu})^2+\Delta^2}-\delta\mu)}{\partial\mu_e}\Big]$$
$$=2(\sqrt{(\sqrt{p_3^2+eBn}-\bar{\mu})^2+\Delta^2}-\delta\mu)$$
$$\Big[\delta(\sqrt{(\sqrt{p_3^2+eBn}-\bar{\mu})^2+\Delta^2}-\delta\mu)(\frac{(\sqrt{p_3^2+eBn}-\bar{\mu})}{6(\sqrt{(\sqrt{p_3^2+eBn}-\bar{\mu})^2+\Delta^2})}-\frac{1}{2})\Big]$$

the integral is

$$2\int_0^\infty \exp-\frac{(p_3^2+eBn)}{\Lambda^2}(\sqrt{(\sqrt{p_3^2+eBn}-\bar{\mu})^2+\Delta^2}-\delta\mu)$$
$$\times\Big[\delta(\sqrt{(\sqrt{p_3^2+eBn}-\bar{\mu})^2+\Delta^2}-\delta\mu)(\frac{(\sqrt{p_3^2+eBn}-\bar{\mu})}{6(\sqrt{(\sqrt{p_3^2+eBn}-\bar{\mu})^2+\Delta^2})}-\frac{1}{2})\Big]dp_3=0$$

for the same reasons then in the gap equation case. Therefore

$$I_3 = \frac{\partial|\sqrt{(\sqrt{p_3^2+eBn}-\bar{\mu})^2+\Delta^2}-\delta\mu|}{\partial\mu_e} = 2\theta(\sqrt{(\sqrt{p_3^2+eBn}-\bar{\mu})^2+\Delta^2}-\delta\mu) \Big[\frac{(\sqrt{p_3^2+eBn}-\bar{\mu})}{6(\sqrt{(\sqrt{p_3^2+eBn}-\bar{\mu})^2+\Delta^2})}-\frac{1}{2}\Big].$$

Hence, simplifying the term I_3 in the same way we did for the potential and rearranging all the terms we get

$$\begin{aligned}
&-\frac{\mu_{db}^3}{9\pi^2}-\frac{eB}{4\pi^2}\sum_{n=0}^{\frac{\mu_e^2}{2eB}}(2-\delta_{n0})\sqrt{\mu_e^2-2eBn}+\frac{eB}{6\pi^2}\sum_{n=0}^{\frac{\mu_{ub}^2}{2eB}}(2-\delta_{n0})\sqrt{\mu_{ub}^2-2eBn}\\
&+\frac{eB}{6\pi^2}\sum_{n=0}^{\infty}(1-\frac{\delta_{n0}}{2})\int_0^{\infty}e^{-}\frac{(p_3^2+eBn)}{\lambda^2}\Big[\frac{\sqrt{p_3^2+eBn}+\bar{\mu}}{\sqrt{(\sqrt{p_3^2+eBn}+\bar{\mu})^2+\Delta^2}}\\
&-\frac{\sqrt{p_3^2+eBn}-\bar{\mu}}{\sqrt{(\sqrt{p_3^2+eBn}-\bar{\mu})^2+\Delta^2}}\Big]dp_3-\frac{eB}{6\pi^2}\times\\
&\theta(\delta\mu-\Delta)\Bigg[\sum_{n_2+1}^{\infty}(1-\frac{\delta_{n0}}{2})\int_0^{\infty}e^{-}\frac{(p_3^2+eBn)}{\lambda^2}\Big(\frac{\sqrt{p_3^2+eBn}-\bar{\mu}}{\sqrt{(\sqrt{p_3^2+eBn}-\bar{\mu})^2+\Delta^2}}-3\Big)dp_3\\
&+\sum_{n=n_1+1}^{n_2}(1-\frac{\delta_{n0}}{2})\int_0^{p_2}e^{-}\frac{(p_3^2+eBn)}{\lambda^2}\Big(\frac{\sqrt{p_3^2+eBn}-\bar{\mu}}{\sqrt{(\sqrt{p_3^2+eBn}-\bar{\mu})^2+\Delta^2}}-3\Big)dp_3\\
&+\sum_{n=0}^{n_1}(1-\frac{\delta_{n0}}{2})\int_{p_1}^{p_2}e^{-}\frac{(p_3^2+eBn)}{\lambda^2}\Big(\frac{\sqrt{p_3^2+eBn}-\bar{\mu}}{\sqrt{(\sqrt{p_3^2+eBn}-\bar{\mu})^2+\Delta^2}}-3\Big)dp_3\Bigg]=0
\end{aligned} \tag{4.21}$$

Color Neutrality Equation

The color neutrality equation

$$\frac{\partial\mu_{db}}{\partial\mu_8}=-\frac{2}{3}$$

can be worked out in a similar way. Taking into account that

$$\frac{\partial\big[\frac{\mu_{ub}}{2}\sqrt{\mu_{ub}^2-2eBn}-eBn\ln(\frac{\sqrt{\mu_{ub}^2-2eBn}+\mu_{ub}}{\sqrt{2eBn}})\big]}{\partial\mu_8}$$
$$=\frac{-2}{3}\big[\frac{1}{2}\sqrt{\mu_{ub}^2-2eBn}+\frac{\mu_{ub}^2}{2\sqrt{\mu_{ub}^2-2eBn}}$$
$$-eBn\frac{(1+\frac{\mu_{ub}}{\sqrt{\mu_{ub}^2-2eBn}})}{\sqrt{\mu_{ub}^2-2eBn}+\mu_{ub}}\big]$$
$$=\frac{-2}{3}\sqrt{\mu_{ub}^2-2eBn}. \tag{4.22}$$

Let us take the partial derivative of last term with respect to μ_8

$$\frac{\partial|\sqrt{(\sqrt{p_3^2+eBn}-\bar{\mu})^2+\Delta^2}-\delta\mu|}{\partial\mu_8}=\frac{2\partial(\sqrt{(\sqrt{p_3^2+eBn}-\bar{\mu})^2+\Delta^2}-\delta\mu)}{\partial\mu_8}$$
$$\Big[\theta(\sqrt{(\sqrt{p_3^2+eBn}-\bar{\mu})^2+\Delta^2}-\delta\mu)\Big]$$
$$+2(\sqrt{(\sqrt{p_3^2+eBn}-\bar{\mu})^2+\Delta^2}-\delta\mu)\Big[\frac{\partial\theta(\sqrt{(\sqrt{p_3^2+eBn}-\bar{\mu})^2+\Delta^2}-\delta\mu)}{\partial\mu_8}\Big].$$

Taking the second term

$$2(\sqrt{(\sqrt{p_3^2+eBn}-\bar{\mu})^2+\Delta^2}-\delta\mu)\Big[\frac{\partial\theta(\sqrt{(\sqrt{p_3^2+eBn}-\bar{\mu})^2+\Delta^2}-\delta\mu)}{\partial\mu_e}\Big]$$
$$=2(\sqrt{(\sqrt{p_3^2+eBn}-\bar{\mu})^2+\Delta^2}-\delta\mu)$$
$$\Big[\delta(\sqrt{(\sqrt{p_3^2+eBn}-\bar{\mu})^2+\Delta^2}-\delta\mu)\frac{\sqrt{p_3^2+eBn}-\bar{\mu}}{3(\sqrt{(\sqrt{p_3^2+eBn}-\bar{\mu})^2+\Delta^2})}\Big]=0$$

the integral becomes

$$2\int_0^\infty \exp-\frac{(p_3^2+eBn)}{\Lambda^2}(\sqrt{(\sqrt{p_3^2+eBn}-\bar{\mu})^2+\Delta^2}-\delta\mu)$$

$$\times\Big[\delta(\sqrt{(\sqrt{p_3^2+eBn}-\bar{\mu})^2+\Delta^2}-\delta\mu)(\frac{(\sqrt{p_3^2+eBn}-\bar{\mu})}{3(\sqrt{(\sqrt{p_3^2+eBn}-\bar{\mu})^2+\Delta^2})})\Big]dp_3$$

Therefore,

$$I_4=\frac{\partial|\sqrt{(\sqrt{p_3^2+eBn}-\bar{\mu})^2+\Delta^2}-\delta\mu|}{\partial\mu_e}=2\theta(\sqrt{(\sqrt{p_3^2+eBn}-\bar{\mu})^2+\Delta^2}-\delta\mu)$$
$$\Big[\frac{(\sqrt{p_3^2+eBn}-\bar{\mu})}{3\sqrt{(\sqrt{p_3^2+eBn}-\bar{\mu})^2+\Delta^2}}\Big].$$

Hence, simplifying the term I_4 in the same way we did for the potential and rearranging all the terms we get

$$\begin{aligned}
&\frac{2\mu_{db}^3}{9\pi^2}+\frac{eB}{6\pi^2}\sum_{n=0}^{\frac{\mu_{ub}^2}{2eB}}(2-\delta_{n0})\sqrt{\mu_{ub}^2-2eBn}\\
&-\frac{eB}{3\pi^2}\sum_{n=0}^{\infty}(1-\frac{\delta_{n0}}{2})\int_0^{\infty}e^{-}\frac{(p_3^2+eBn)}{\lambda^2}\Big[\frac{\sqrt{p_3^2+eBn}+\bar{\mu}}{\sqrt{(\sqrt{p_3^2+eBn}+\bar{\mu})^2+\Delta^2}}\\
&-\frac{\sqrt{p_3^2+eBn}-\bar{\mu}}{\sqrt{(\sqrt{p_3^2+eBn}-\bar{\mu})^2+\Delta^2}}\Big]dp_3\\
&+\frac{eB}{3\pi^2}\theta(\delta\mu-\Delta)\Bigg[\sum_{n_2+1}^{\infty}(1-\frac{\delta_{n0}}{2})\int_0^{\infty}e^{-}\frac{(p_3^2+eBn)}{\lambda^2}\frac{\sqrt{p_3^2+eBn}-\bar{\mu}}{\sqrt{(\sqrt{p_3^2+eBn}-\bar{\mu})^2+\Delta^2}}dp_3\\
&+\sum_{n=n_1+1}^{n_2}(1-\frac{\delta_{n0}}{2})\int_0^{p_2}e^{-}\frac{(p_3^2+eBn)}{\lambda^2}\frac{\sqrt{p_3^2+eBn}-\bar{\mu}}{\sqrt{(\sqrt{p_3^2+eBn}-\bar{\mu})^2+\Delta^2}}dp_3\\
&+\sum_{n=0}^{n_1}(1-\frac{\delta_{n0}}{2})\int_{p_1}^{p_2}e^{-}\frac{(p_3^2+eBn)}{\lambda^2}\frac{\sqrt{p_3^2+eBn}-\bar{\mu}}{\sqrt{(\sqrt{p_3^2+eBn}-\bar{\mu})^2+\Delta^2}}dp_3\Bigg]=0.
\end{aligned}\tag{4.23}$$

4.2 Chromomagnetic Instability

To explore the stability of the 2SC phase, the numerical calculation of the Meissner screening mass of the gluons was done in [28] for a system at zero magnetic field. In that work, they studied the Meissner masses squared as function of $\frac{\Delta}{\delta\mu}$ at different temperatures. Their results show that the square of the screening mass of $8th$ gluon is negative for $\frac{\Delta}{\delta\mu} < 1$, this is the gapless region of 2SC. There is another type of instability associated to the charged gluons with color index 4 to 7 This instability exists in both g2SC and 2SC phases in the region $\frac{\Delta}{\delta\mu} < \sqrt{2}$. In the region $\delta\mu < \Delta < \sqrt{2}\delta\mu$, the Meissner masses of the four charged gluons become imaginary, indicating the ground state is not the correct one.

The work of [30] also shows that at $T = 0$ K, the g2SC phase exists in the region

$$92 \text{ MeV} < \Delta_0 < 134 \text{ MeV},$$

and the 2SC phase for

$$\Delta_0 > 134 \text{ MeV}$$

for quark chemical potential $\mu = 400$ MeV. There it has also been emphasized that for extremely strong couplings, $\Delta_0 \geq 162$ MeV, the 2SC phase is free from instability.

Although the negative values of the screening masses of gluons give the signature of chromomagnetic instability in the di-quark ground state, no work has been done yet to explore such instability in the presence of a magnetic field. However, before attempting such a study, one needs to investigate the relation between the gap and the mismatch parameter $\delta\mu$. In this work we carry out such an investigation. As we will see, a magnetic field can increase the gap enough to

take it out of the unstable region $\delta\mu < \Delta < \sqrt{2}\delta\mu$ for a fixed interaction strength and density.

Chapter 5

Results and Discussion

In this chapter we present the numerical findings of this work for arbitrary field values. We find the gap solution and the chemical potential solutions as function of the magnetic field. For consistency, we compare our results with those of [31] and [27] at strong field and in at zero field respectively.

5.1 Numerical Solution for the Gap and Chemical Potentials

As derived earlier rewriting the gap Eq.4.17

$$\frac{\Delta}{2G} - \frac{eB\Delta}{\pi^2}\sum_{n=0}^{\infty}(1-\frac{\delta_{n0}}{2})\int_0^{\infty} e^{-}\frac{(p_3^2+eBn)}{\lambda^2}\Big[\frac{1}{\sqrt{(\sqrt{p_3^2+eBn}+\bar{\mu})^2+\Delta^2}} + \frac{1}{\sqrt{(\sqrt{p_3^2+eBn}-\bar{\mu})^2+\Delta^2}}\Big]dp_3$$
$$+\theta(\delta\mu-\Delta)\frac{eB\Delta}{\pi^2}\Big[\sum_{n=n_2+1}^{\infty}(1-\frac{\delta_{n0}}{2})\int_0^{\infty}\frac{e^{-\frac{(p_3^2+eBn)}{\lambda^2}}}{\sqrt{(\sqrt{p_3^2+eBn}-\bar{\mu})^2+\Delta^2}}$$
$$+\sum_{n=n_1+1}^{n_2}(1-\frac{\delta_{n_0)}}{2}\int_{p_2}^{\infty}\frac{e^{-\frac{(p_3^2+eBn)}{\lambda^2}}}{\sqrt{(\sqrt{p_3^2+eBn}-\bar{\mu})^2+\Delta^2}}$$

$$+\sum_{n=0}^{n_1}(1-\frac{\delta_{n0}}{2})\int_{p_1}^{p_2}\frac{e^{-\frac{(p_3^2+eBn)}{\lambda^2}}}{\sqrt{(\sqrt{p_3^2+eBn}-\bar{\mu})^2+\Delta^2}}\Big]dp_3$$
$$=0. \qquad (5.1)$$

To solve this equation we consider the momentum cutoff $\Lambda = 653.3$ MeV and quark chemical potential $\mu = 400$ MeV which are typical values for the 2SC phase. We have another parameter the coupling constant G which significantly can influence the gap solution. For certain values of G, the values of Δ become larger than $\delta\mu$ and for others it is less than $\delta\mu$. It has been shown in [27] that at zero magnetic field there are two phases of 2SC superconductors, depending upon whether $\Delta >$ or $< \delta\mu$. $\Delta > \delta\mu$ is the gapped phase and the other one $\Delta < \delta\mu$ is the gapless one. Here we have set the values of $G > 4.5 \times 10^{-6}$ MeV^2 for which the gap exceeds the value of $\delta\mu$. So we are working in the gapped region. The fixing of these physical constants is done in a way that we can recover the zero field value of the gap. While choosing these values of the coupling constant, we need to be careful what type of cutoffs are being used. There are several choices of such cutoffs, such as: sharp and smooth cutoffs. After several trials, we found that the smooth Gaussian cutoff is better suited to work with a finite magnetic field in numerical calculations and therefore this is the one considered here.

Our problem requires to solve a set of three coupled equations with three unknowns Δ, μ_e and μ_8. These are the gap equation and the two neutrality conditions. The neutrality conditions are

$$-\frac{\mu_{db}^3}{9\pi^2}-\frac{eB}{4\pi^2}\sum_{n=0}^{\frac{\mu_e^2}{2eB}}(2-\delta_{n0})\sqrt{\mu_e^2-2eBn}+\frac{eB}{6\pi^2}\sum_{n=0}^{\frac{\mu_{ub}^2}{2eB}}(2-\delta_{n0})\sqrt{\mu_{ub}^2-2eBn}$$
$$+\frac{eB}{6\pi^2}\sum_{n=0}^{\infty}(1-\frac{\delta_{n0}}{2})\int_0^{\infty}e^{-\frac{(p_3^2+eBn)}{\lambda^2}}\Big[\frac{\sqrt{p_3^2+eBn}+\bar{\mu}}{\sqrt{(\sqrt{p_3^2+eBn}+\bar{\mu})^2+\Delta^2}}$$

$$
\begin{aligned}
&-\frac{\sqrt{p_3^2+eBn}-\bar{\mu}}{\sqrt{(\sqrt{p_3^2+eBn}-\bar{\mu})^2+\Delta^2}}\Big]dp_3-\frac{eB}{6\pi^2}\times\\
\theta(\delta\mu-\Delta)\Bigg[&\sum_{n_2+1}^{\infty}(1-\frac{\delta_{n0}}{2})\int_0^{\infty}e^{-}\frac{(p_3^2+eBn)}{\lambda^2}\Big(\frac{\sqrt{p_3^2+eBn}-\bar{\mu}}{\sqrt{(\sqrt{p_3^2+eBn}-\bar{\mu})^2+\Delta^2}}-\frac{3}{1}\Big)dp_3\\
&+\sum_{n=n_1+1}^{n_2}(1-\frac{\delta_{n0}}{2})\int_0^{p_2}e^{-}\frac{(p_3^2+eBn)}{\lambda^2}\Big(\frac{\sqrt{p_3^2+eBn}-\bar{\mu}}{\sqrt{(\sqrt{p_3^2+eBn}-\bar{\mu})^2+\Delta^2}}-\frac{3}{1}\Big)dp_3\\
&+\sum_{n=0}^{n_1}(1-\frac{\delta_{n0}}{2})\int_{p_1}^{p_2}e^{-}\frac{(p_3^2+eBn)}{\lambda^2}\Big(\frac{\sqrt{p_3^2+eBn}-\bar{\mu}}{\sqrt{(\sqrt{p_3^2+eBn}-\bar{\mu})^2+\Delta^2}}-\frac{3}{1}\Big)dp_3\Bigg]=0
\end{aligned}
\tag{5.2}
$$

and

$$
\begin{aligned}
&\frac{2\mu_{db}^3}{9\pi^2}+\frac{eB}{6\pi^2}\sum_{n=0}^{\frac{\mu_{ub}^2}{2eB}}(2-\delta_{n0})\sqrt{\mu_{ub}^2-2eBn}\\
&-\frac{eB}{3\pi^2}\sum_{n=0}^{\infty}(1-\frac{\delta_{n0}}{2})\int_0^{\infty}e^{-}\frac{(p_3^2+eBn)}{\lambda^2}\Big[\frac{\sqrt{p_3^2+eBn}+\bar{\mu}}{\sqrt{(\sqrt{p_3^2+eBn}+\bar{\mu})^2+\Delta^2}}\\
&-\frac{\sqrt{p_3^2+eBn}-\bar{\mu}}{\sqrt{(\sqrt{p_3^2+eBn}-\bar{\mu})^2+\Delta^2}}\Big]dp_3\\
+\frac{eB}{3\pi^2}\theta(\delta\mu-\Delta)\Bigg[&\sum_{n_2+1}^{\infty}(1-\frac{\delta_{n0}}{2})\int_0^{\infty}e^{-}\frac{(p_3^2+eBn)}{\lambda^2}\frac{\sqrt{p_3^2+eBn}-\bar{\mu}}{\sqrt{(\sqrt{p_3^2+eBn}-\bar{\mu})^2+\Delta^2}}dp_3\\
&+\sum_{n=n_1+1}^{n_2}(1-\frac{\delta_{n0}}{2})\int_0^{p_2}e^{-}\frac{(p_3^2+eBn)}{\lambda^2}\frac{\sqrt{p_3^2+eBn}-\bar{\mu}}{\sqrt{(\sqrt{p_3^2+eBn}-\bar{\mu})^2+\Delta^2}}dp_3\\
&+\sum_{n=0}^{n_1}(1-\frac{\delta_{n0}}{2})\int_{p_1}^{p_2}e^{-}\frac{(p_3^2+eBn)}{\lambda^2}\frac{\sqrt{p_3^2+eBn}-\bar{\mu}}{\sqrt{(\sqrt{p_3^2+eBn}-\bar{\mu})^2+\Delta^2}}dp_3\Bigg]=0.
\end{aligned}
\tag{5.3}
$$

Large Magnetic Field

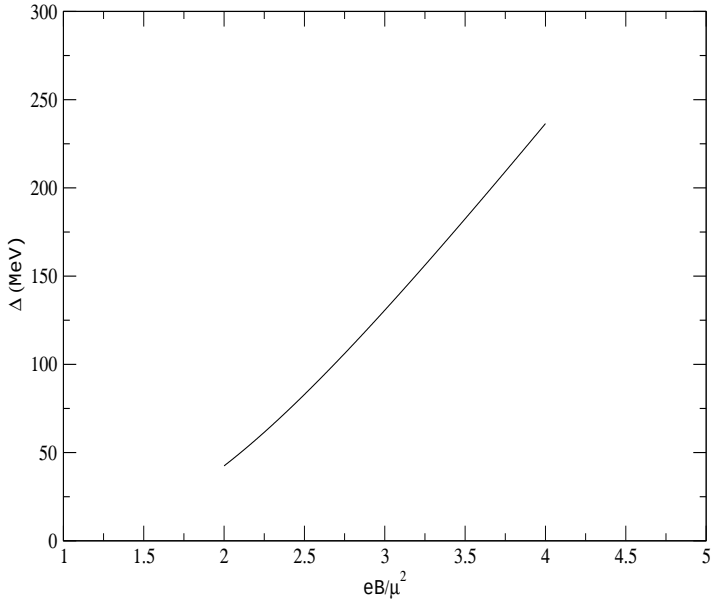

Figure 5.1: Variation of gap of 2SC with magnetic field at coupling constant $G = 5.0 \times 10^{-6}$ MeV^{-2}.

The analytical solutions of the Eqs.4.17-5.3 in the gapped phase at large magnetic fields were found in [31]. Although our main goal in this thesis is to explore the more interesting region of intermediate magnetic fields, we decided to start our work by testing our numerical technique by considering the strong magnetic field case. This will allow us to compare our results for the gap and chemical potentials with the analytical findings of [31]. Then, in this strong field regime, we considered the three equations with no assumption about the magnitude of the gap or the chemical potentials.

The density of states available for Cooper pairs is a function of the magnetic field; if a magnetic field is raised so will the density of states. As a consequence

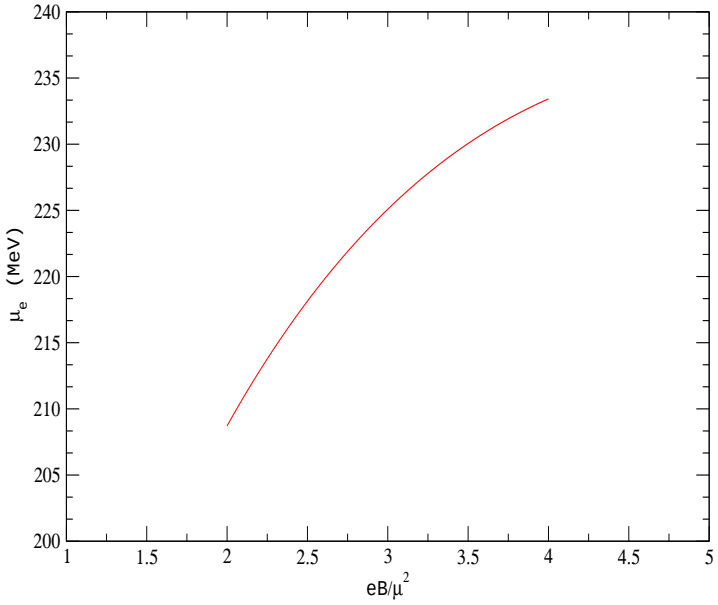

Figure 5.2: Variation of μ_e of 2SC with magnetic field at coupling constant $G = 5.0 \times 10^{-6}$ MeV^{-2}.

of this the quarks participating in the pairing lie all at the zero Landau level for large enough fields. We can therefore reduce the sum over Landau levels to only $n = 0$, which makes the problem straightforward to solve analytically as was done in [31]. If one is interested in reproducing those results numerically, it is possible to use a sharp cutoff, since the problems related to the Landau level sum are not present here because only the zero Landau level contributes at very large fields. We study the variation of the gap computationally and compare with the result shown in [31]. Fig. 5.1 shows our numerical result in this strong field region. It is consistent with the analytical result obtained in [31].

We also compare the results for electric and color charge chemical potentials, i.e., μ_e and μ_8. Fig. 5.2 and 5.3 also show a similar agreement between our calculated and analytical results as it is seen in the case of gap.

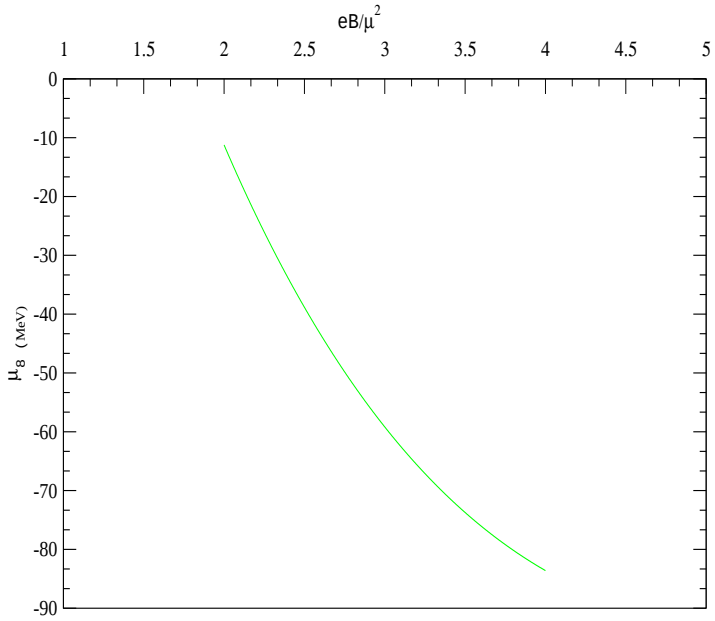

Figure 5.3: Variation of μ_8 of 2SC with magnetic field at coupling constant $G = 5.0 \times 10^{-6}$ MeV^{-2}.

Arbitrary Magnetic Field

As we see from the above results the magnitude of μ_8 is comparable with Δ and μ_e only for large magnetic fields. For arbitrary but intermediate magnetic fields, the region of interest in the present subsection, we can then neglect μ_8, as it will be much smaller than the gap and the electric chemical potential. It is more convenient to work with a combination of the electric and color neutrality conditions and take the approximation $\mu_8 = 0$ there and in the gap equation. Then, the neutrality condition reduces to

$$n_Q + \frac{1}{2}n_8 = -\frac{eB}{4\pi^2}\sum_{n=0}^{\frac{\mu_e^2}{2eB}}(2-\delta_{n0})\sqrt{\mu_e^2 - 2eBn} - \frac{eB}{4\pi^2}\sum_{n=0}^{\frac{\mu_{ub}^2}{2eB}}(2-\delta_{n0})\sqrt{\mu_{ub}^2 - 2eBn} = 0. \tag{5.4}$$

We then solve these two equations Eq.5.1 and Eq.5.4. We perform the numerical computation of the gap and the electric potential in a range of magnetic fields $0.1 < \frac{eB}{2\mu^2} < 2$. At $G = 4.76 \times 10^{-6}$ MeV^2, the variation of Δ normalized to Δ_0 with $\frac{eB}{\mu^2}$ is shown in Fig.5.4. Here Δ_0 represents the gap at zero field for the same values of coupling constant G, cutoff and baryonic chemical potential μ. We see that the gap is oscillating with the magnetic field within the region $\frac{eB}{\mu^2} = 0.16$ to 1.5 . If we move towards a smaller magnetic field value i.e., $\frac{eB}{\mu^2} \leq 0.16$, the gap oscillations are too small to be observed and tends to its zero field value. At small magnetic field the sum over Landau levels can be replaced by a integral, therefore the gap goes to its zero field limit. If we approach $\frac{eB}{\mu^2} > 2$, the gap is no longer oscillating because it hits the region where only the lowest LL contributes.

Unlike the gap, in this case, however the electric chemical potential μ_e is independent of the magnetic field. This is because its field dependence would come

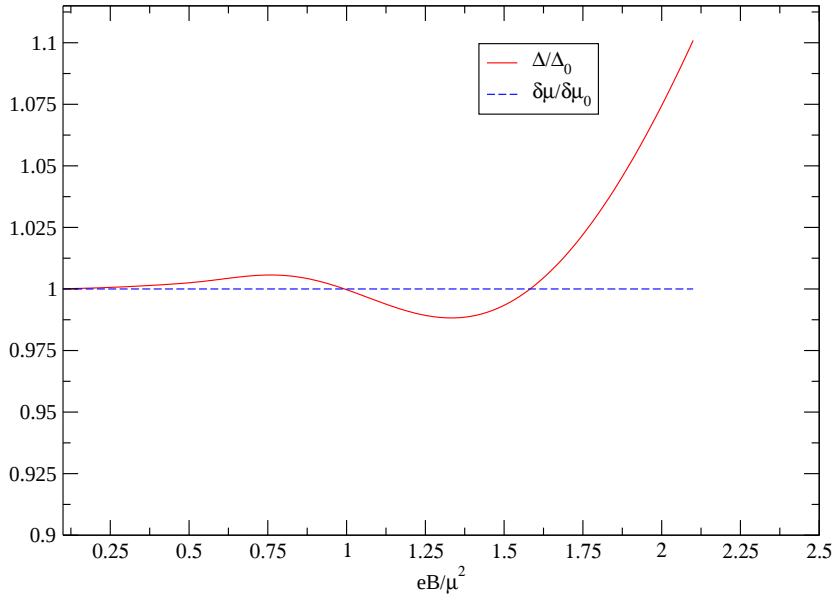

Figure 5.4: Variation of gap of 2SC with magnetic field at coupling constant $G = 4.76 \times 10^{-6}$ MeV^{-2}

only from μ_8 which has been neglected in the calculation.

5.2 Magnetic-field Induced Stability

Here we discuss the variation of the gap with the magnetic field for different

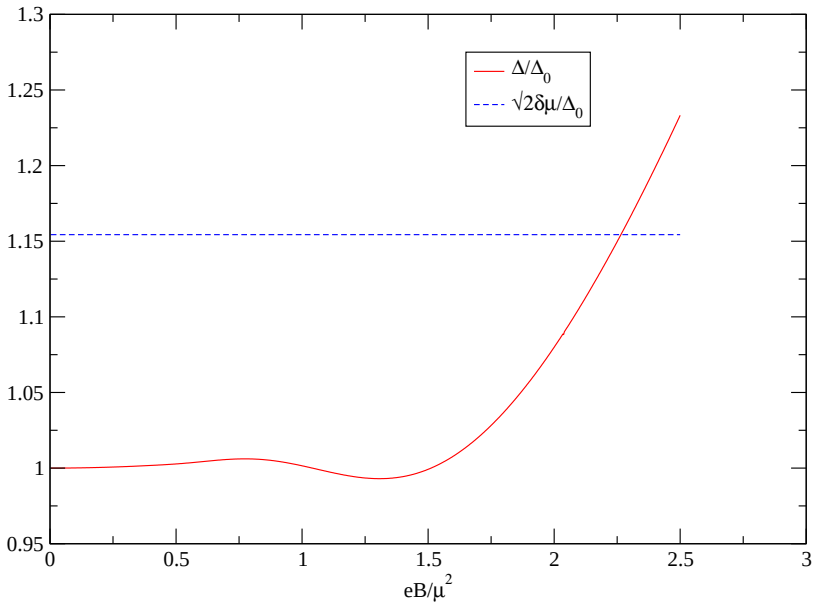

Figure 5.5: Variation of gap of 2SC with magnetic field at coupling constant $G = 4.80 \times 10^{-6}$ MeV^{-2}

.

values of the coupling constant and compare the di-quark stability regions associated with them. Fig.5.5 shows the magnetic field dependence of $\frac{\Delta}{\Delta_0}$ and the horizontal line $\sqrt{2}\delta\mu$ at $G = 4.80 \times 10^{-6}$ MeV^{-2}. The region below the dotted line refers to an unstable region and the region above that line is a stable region as indicated by the imaginary screening mass of gluons [30] favored at $B = 0$. Here we see that at this coupling constant, the gap also exhibits unstable

behavior in the region $\frac{eB}{\mu^2} = 0.16$ to 2.0. It crosses the stability line at $\frac{eB}{\mu^2} > 2.0$.

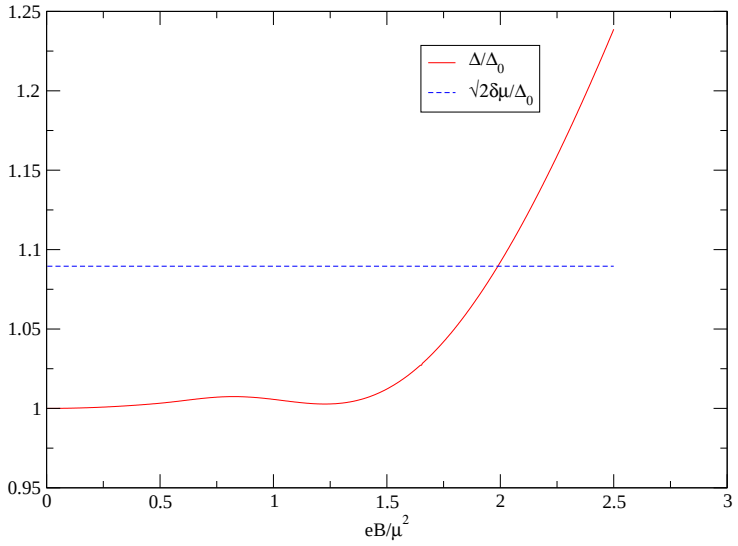

Figure 5.6: Variation of gap of 2SC with magnetic field at coupling constant $G = 4.90 \times 10^{-6}$ MeV^{-2}

Fig.5.6 refers to the variation of gap with magnetic field at $G = 4.90 \times 10^{-6}$ MeV^{-2}. In this case, the gap crosses the stability line for $\frac{eB}{\mu^2} < 2$. This implies that an increase in the coupling constant enhances the gap and hence the stability.

Fig.5.7 refers to the variation of the gap with the magnetic field at $G = 5.0 \times 10^{-6}$ MeV^{-2}. In this case, the gap crosses the stability line for $\frac{eB}{\mu^2} << 2$. It also shows same trend in the gap, i.e., it takes the di-quark gap to a stable region even at lower magnetic field.

Fig.5.8 refers to the variation of the gap with the magnetic field at $G = 5.05 \times 10^{-6}$ MeV^{-2}. In this case, the gap lies in the unstable gapped region, but very close to the stability line. Under such conditions the oscillations are enough to induce stability themselves, as can be seen by the crossing at $\frac{eB}{\mu^2} \approx 0.5$. In this case, after crossing at a much smaller field, the gap keeps increasing with the

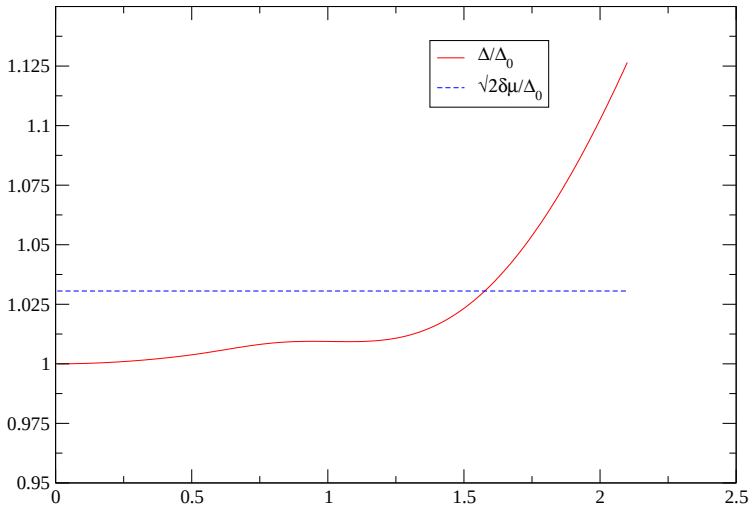

Figure 5.7: Variation of gap of 2SC with magnetic field at coupling constant $G = 5.0 \times 10^{-6}$ MeV^{-2}

field, thereby remaining in the stable region of a much larger range of magnetic fields.

A comparison of Figs. 5.5 and 5.8 shows that the effect of the field on the gap is quite sensitive to the coupling strength. For instance, a 2% increase in in the coupling produces a 7% increase in the gap and a 25% decrease in the field required to induce the crossing to the stable region.

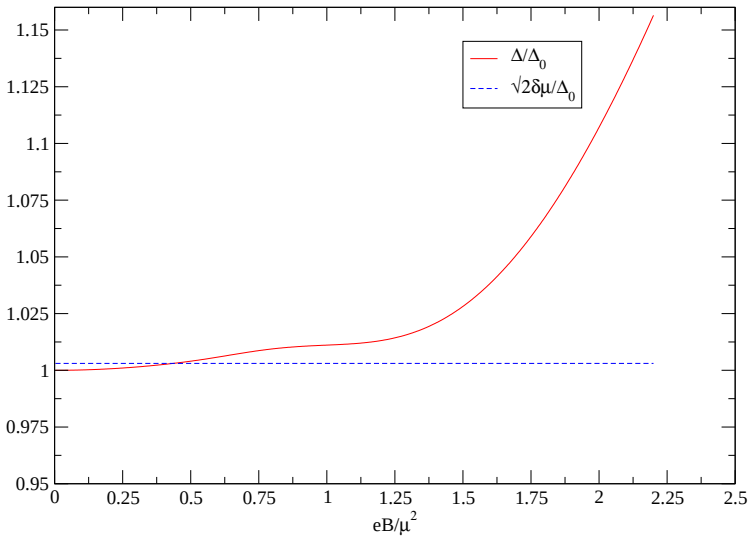

Figure 5.8: Variation of gap of 2SC with magnetic field at coupling constant $G = 5.05 \times 10^{-6}$ MeV^{-2}

Chapter 6

Concluding Remarks

In the present work, we studied the effects of a magnetic field on the 2SC phase of color superconductivity. In the first part of this thesis work, we developed analytic expressions for the gap and neutrality equations that allowed us to explore the strong magnetic field behavior in the unstable and stable regions of the gapped 2SC phase and helped us to prepare the equations in a more convenient form for the numerical studies of the second part. In the second part of our work we undertook a numerical study of the equations at arbitrary values of the magnetic field. Our study explored the unstable gapped region $\delta\mu < \Delta < \sqrt{2}\delta\mu$. Our results show that at strong enough field, the gap increases exponentially with the field. This is the consequence of the occupancy of the lowest Landau level by all the charged particles at large fields, which in turn is reflected in the density of states entering in the gap analytical solution. This fact is analogous to the exponential behavior of the gap with the density of states in the case of conventional superconductivity.

For field values in the range $0 \leq \tilde{e}\tilde{B} \leq 2\mu^2$ the gap exhibits an oscillating behavior. This behavior has similarity to the three-flavor MCFL phase, these oscillations are associated with the de Hass Van Alphen effect that occurs with changing field when Landau levels (LL) become either emptied or filled. The dis-

crete character of the LL and the change of the density of states of each level with the field is reflected in the oscillating behavior of the thermodynamic potential and hence in various physical quantities as the gap, magnetization, etc. At small field the oscillations are too small to be seen in the graph. They become more prominent in the range $0.25\mu^2 < \tilde{e}\tilde{B} < 1.5\mu^2$, depending on the strength of the coupling. Once $\tilde{e}\tilde{B} > 2\mu^2$, the gap starts to increase because the quarks in the pairing are all in the lowest Landau level (LLL).

The most relevant result we have found in the present work is the observed tendency of the field to take the gap out of the unstable region, an effect that is clearly shown in Figs. 5.6, 5.7 and 5.8. At stronger coupling, the field-induced stability is reached for smaller fields (see Fig.5.8). We studied the gap for different values of the coupling constant and found that it is very sensitive to the coupling strength. In our case we considered only those values which give gap Δ greater than the mismatch parameter $\delta\mu$ as we were interested in the possible effect of the magnetic field on the region of instability.

An interesting next step worth of a PhD level thesis will be to calculate the Meissner masses of the charged gluons in the 2SC phase in the presence of a magnetic field. We expect that the stability tendency found in our work will be reflected in real gluon masses in the region of the parameter space that was found to be unstable at zero magnetic field.

Bibliography

[1] Krishna Rajagopal and Frank Wilczek. The condensed matter physics of QCD. *arXiv:hep-ph/0011333*, 2000.

[2] D. J. Gross and Frank Wilczek. Ultraviolet behavior of non-abelian gauge theories. *Phys. Rev. Lett.*, 30:1343–1346, 1973.

[3] Mark G. Alford, Andreas Schmitt, Krishna Rajagopal, and Thomas Schafer. Color superconductivity in dense quark matter. *Rev. Mod. Phys.*, 80:1455–1515, 2008.

[4] Igor A. Shovkovy. Color superconductivity in dense quark matter. *arXiv:nucl-th/0511014*, 2005.

[5] Mark Alford, Chris Kouvaris, and Krishna Rajagopal. Evaluating the Gapless Color-Flavor Locked Phase. *Phys. Rev.*, D71:054009, 2005.

[6] Mark G. Alford, Krishna Rajagopal, and Frank Wilczek. QCD at finite baryon density: Nucleon droplets and color superconductivity. *Phys. Lett.*, B422:247–256, 1998.

[7] Juergen Berges and Krishna Rajagopal. Color superconductivity and chiral symmetry restoration at nonzero baryon density and temperature. *Nucl. Phys.*, B538:215–232, 1999.

[8] Igor A. Shovkovy. Two lectures on color superconductivity. *Found. Phys.*, 35:1309–1358, 2005.

[9] Charles. Kittel. *Introduction to Solid State Physics*. John Wiley and Sons, Inc., 8th edition, 2005.

[10] J. Bardeen, L. N. Cooper, and J. R. Schrieffer. Theory of Superconductivity. *Phys. Rev.*, 108(5):1175–1204, Dec 1957.

[11] James M. Lattimer and Maddapa Prakash. Neutron Star Observations: Prognosis for Equation of State Constraints. *Phys. Rept.*, 442:109–165, 2007.

[12] Bertrand C. Barrois. Superconducting Quark Matter. *Nucl. Phys.*, B129:390, 1977.

[13] D. Bailin and A. Love. Superfluidity and Superconductivity in Relativistic Fermion Systems. *Phys. Rept.*, 107:325, 1984.

[14] Steven C. Frautschi. Summary talk: hadronic interaction session. Presented at 13th Rencontre de Moriond, Les Arcs, France, Mar 12-18, 1978.

[15] D. Bailin and A. Love. Superfluid quark matter. *J. Phys.*, A12:L283, 1979.

[16] R. Rapp, Thomas Schafer, Edward V. Shuryak, and M. Velkovsky. Diquark Bose condensates in high density matter and instantons. *Phys. Rev. Lett.*, 81:53–56, 1998.

[17] Mark G. Alford, Krishna Rajagopal, and Frank Wilczek. Color-flavor locking and chiral symmetry breaking in high density QCD. *Nucl. Phys.*, B537:443–458, 1999.

[18] Efrain J. Ferrer, Vivian de la Incera, and Cristina Manuel. Magnetic color flavor locking phase in high density QCD. *Phys. Rev. Lett.*, 95:152002, 2005.

[19] Efrain J. Ferrer, Vivian de la Incera, and Cristina Manuel. Color-superconducting gap in the presence of a magnetic field. *Nucl. Phys.*, B747:88–112, 2006.

[20] G. Chanmugam. Magnetic fields of degenerate stars. *Ann. Rev. Astron. Astrophys.*, 30:143–184, 1992.

[21] Christopher Thompson and Robert C. Duncan. The Soft gamma repeaters as very strongly magnetized neutron stars. 2. Quiescent neutrino, x-ray, and Alfven wave emission. *Astrophys. J.*, 473:322, 1996.

[22] D. Lai and S. L. Shapiro. Cold equation of state in a strong magnetic field - Effects of inverse beta-decay. *APJ*, 383:745–751, Dec 1991.

[23] Efrain J. Ferrer, Vivian de la Incera, Jason P. Keith, Israel Portillo, and Paul P. Springsteen. Equation of State of a Dense and Magnetized Fermion System. *Phys. Rev.*, C82:065802, 2010.

[24] Kenji Fukushima and Harmen J. Warringa. Color superconducting matter in a magnetic field. *Phys. Rev. Lett.*, 100:032007, 2008.

[25] Jorge L. Noronha and Igor A. Shovkovy. Color-flavor locked superconductor in a magnetic field. *Phys. Rev.*, D76:105030, 2007.

[26] M. Huang, P. F. Zhuang and W. Q. Chao, Phys. Rev. D **67**, 065015 (2003)

[27] Mei Huang and Igor Shovkovy. Gapless color superconductivity at zero and at finite temperature. *Nucl. Phys.*, A729:835–863, 2003.

[28] Mei Huang and Igor A. Shovkovy. Screening masses in neutral two-flavor color superconductor. *Phys.Rev.*, D70:094030, 2004.

[29] Kei Iida and Kenji Fukushima. Instability of a gapless color superconductor with respect to inhomogeneous fluctuations. *Nucl.Phys.*, A785:118–121, 2007.

[30] O. Kiriyama. Meissner screening mass in two-flavor quark matter at nonzero temperature. *Phys. Rev.*, D74:074019, 2006.

[31] Thomas James Topel. 2SC color superconductivity in a magnetic field. Master's thesis, Department of Physics of Western Illinois University, 2008.

Curriculum Vita

Churna B Bhandari was born and raised in Nepal, Phulbari on 14 September 1981, the son of Asha Ram Bhandari and Shanta Bhandari. He received his Bachelor degree of science from Trichandra College. He also earned his Master degree of Science Solid State Physics as a major from the Tribhuvan University of Nepal. In 2007 he was assigned as a part-time lecturer of Spectroscopy for M.Sc. first year students in the Physics Department. He got a fellowship as an outstanding young physicist from a developing country at Abdus Salam International Centre for Theoretical Physics to participate in an advanced Pre-Ph.D. level Diploma course of Condensed Matter Physics in September, 2008. After successful completion of Diploma course, he joined the Physics Department at UTEP in September, 2009 as a graduate student for Master degree of science. During his study at UTEP, he carried research work in the color superconductivity.